UPGRADING AGBABU BITUMEN USING HYDROUS AND ANHYDROUS PYROLYSIS

BY

RAJI, Abdulkadiri
MEng/SEET/2017/6854

DEPERTMENT OF CHEMICAL ENGINEERING
FEDERAL UNIVERSITY OF TECHNOLOGY,
MINNA

NOVEMBER, 2021

ABSTRACT

With the increasing scarcity of conventional crude oil, a consequence of depletion and decline in production due to the fact that petroleum is extracted much faster than its rate of formation, there is need to source for crude oil from the unconventional sources such as oil sand, oil shale and bitumen. However, heavy oils cannot be transported easily without first upgrading. This thesis was undertaken to evaluate Agbabu bitumen as feedstock for synthetic crude oil production via pyrolysis. Initial characterization tests were carried out on the bitumen including Thermogravimetric Analysis (TGA), Fourier Transform Infrared Spectroscopy (FT-IR), Scanning Electron Microscopy (SEM) and Gas Chromatography Mass Spectrometry (GC-MS) to determine the thermal behaviour, functional groups, elemental composition and nature of the Saturates, Aromatics, Resins and Asphaltenes (SARA) composition of the bitumen. Bitumen pyrolysis (Anhydrous pyrolysis) and Bitumen-water mixture pyrolysis (Hydrous pyrolysis) were carried out using a horizontal tube furnace at different temperatures from 200 ^{o}C to 500 ^{o}C and time from 30 minutes to 60 minutes. Design Expert was used to obtain the optimum condition for the pyrolysis experiments with temperature and time set as variables. The synthetic crude oil obtained from both processes were subjected to further test to determine the viscosity, density, specific gravity, determination of the API gravity and GC-MS analysis. The bitumen was found to have high viscosity of 28 cSt and low API gravity of 8.6 ^{o}API which corresponds to standard for heavy oil. The bitumen SARA components determined are 35 % saturates, 37 % aromatics, 26 % resins and 2 % asphaltenes. At the end of the study, it was established that the yield of synthetic crude oil from hydrous pyrolysis has a greater API gravity of 29.20, lower viscosity 3.04 cSt and a higher concentration of saturates 65 % than the synthetic crude obtained from anhydrous pyrolysis which respectively had 23.99, 0.16 %, 3.28 cSt and 50 %. Kinetic studies were carried out from the TGA for both hydrous and anhydrous pyrolysis using Coats-Redfern Method. The activation energy for anhydrous pyrolysis was 291.796 kJmol^{-1} which was higher than that of hydrous pyrolysis 224.04 kJmol^{-1}. Hence hydrous pyrolysis proceeds at a much faster rate and it requires less energy input than anhydrous pyrolysis.

CHAPTER ONE

1.0 INTRODUCTION

1.1 Background to the Study

Petroleum has become the world's most important source of energy as it is used in supplying energy to power industries, generate electricity, heat homes and provide fuel for vehicles and airplanes to carry goods and people all over the world. Also refined products of petroleum are used to manufacture almost all chemical products, such as plastics, fertilizers, detergents and paints. However, there is an increasing scarcity of conventional oil reserves due to depletion and decline in production as argued in the studies of Dr. Marion King Huppert (Meredith *et al*., 2012) based on the fact that petroleum is extracted much faster than its rate of formation, hence the need to source for unconventional crude oil becomes imperative. The unconventional sources of crude oil are oil-shale, heavy oil and oil-sands. Ondo State has one of the largest deposits of bitumen in the whole world and these have not been exploited for petroleum production (Ogunsuyi *et al*., 2011).

When heat leads to the decomposition of organic matter in absence of oxygen it is termed Pyrolysis. There are two types of pyrolysis: Hydrous pyrolysis where the heated material is in contact with water and Anhydrous pyrolysis which is thermal decomposition in inert environment. The general name for all Hydrothermal pyrolysis processes with water either in the liquid phase, vapour phase or steam is Aquathermolysis. Hydrous Pyrolysis provides a means of acquiring information relating to stages, kinetics and indices of petroleum generation that would be difficult to obtain from a study of only the natural system (Pan *et al*., 2012).

The effects of water on hydrocarbon generation and source rock maturation are (a) Pyrolysate from hydrous pyrolysis are more physically, chemically and isotopically similar to crude oils obtained from natural maturation conditions as in catagenesis (Pomerantz *et al*., 2013). (b) Hydrous pyrolysis has also shown to increase gas generation and the pyrolysate yield and reduce maturation time (Lewan *et al*., 2018).

1.2 Statement of Research Problem

Nigeria has an estimated 38 billion barrels of extra-heavy oil and bitumen reserves (Ogundele *et al.,* 2019) and these are virtually unexploited for crude oil production purposes. The increasing scarcity of conventional oil reserves calls for the need to explore unconventional sources of crude oil such as oil shale, oil sand and bitumen. There is little or no information about the kinetics of hydrous pyrolysis of Nigerian bitumen (Ogunsuyi *et al.,* 2011).

1.3 Justification of the Research

Bitumen contains oil rich hydrocarbons (saturates) and it can be subjected to pyrolysis (either hydrous or anhydrous) to produce crude oil. Subjecting bitumen to anhydrous pyrolysis will yield crude oil, however the crude oil yields from hydrous pyrolysis are more physically, chemically and isotopically similar to crude oils obtained from natural maturation conditions as in catagenesis (Berwick *et al.,* 2017). There is abundance of Bitumen in Ondo State; the largest deposit of Bitumen in Africa (Ogundele *et al.,* 2019).

1.4 Aim and Objectives of the Study

The aim of this study is to evaluate Agbabu bitumen as feedstock for synthetic crude oil production via pyrolysis.

This aim will be achieved by carrying out the following objectives:

1. Characterization of the bitumen: TGA, GC-MS, SEM, FT-IR, viscosity, density and specific gravity.
2. Anhydrous pyrolysis at different temperatures 200 ˚C, 250 ˚C, 300 ˚C, 350 ˚C and 400 ˚C for periods of 30 minutes, 45 minutes and 60 minutes using RSM Design Expert.
3. Hydrous Pyrolysis at different temperatures 300 ˚C, 350 ˚C, 400 ˚C, 450 ˚C and 500 ˚C for periods of 30 minutes, 45 minutes and 60 minutes using RSM Design Expert.
4. Determination of the compositions of the synthetic crude oil yields from both pyrolysis processes using GC-MS.
5. Kinetic studies using Coats-Redfern Method.

1.5 Scope of the Research

The scope of this study covers characterization of Bitumen, collected from Agbabu which is situated in Odigbo Local Government Area of Ondo State, using TGA, GC-MS, SEM, FT-IR, viscosity, density and specific gravity of the Bitumen, Hydrous and Anhydrous pyrolysis of the Bitumen at different temperatures and different time intervals to produce pyrolysate using the 1200-Degree lab-scale Nitrogen atmosphere horizontal tubular pyrolysis equipment and determination of the compositions of the synthetic crude oil yields using GC-MS.

CHAPTER TWO

2.0 LITERATURE REVIEW

Hydrocarbon exploration during the last twenty years has increasingly targeted high pressure deep water geological basins. The geochemical models devised to predict source rock maturity and hydrocarbon generation assume that temperature and geological time are the controlling parameters during hydrocarbon generation and source rock maturation, with pressure having no significant effect (Lewan *et al*., 2018). Most high pressure confined pyrolysis studies using gold bags or capsules as the reaction cell either under anhydrous (absence of water) or hydrous (presence of water) conditions have shown that pressure has minimal (Shabbar *et al*., 2018), insignificant (Uguna *et al*., 2012), enhancing or retarding effect on hydrocarbon generation and maturation reactions. On the other hand, high pressure hydrous pyrolysis experiments which more closely resemble natural conditions have shown pressure retardation of hydrocarbon generation and source rock maturation (Wampler, 2007). In geological basins source rock/kerogen, bitumen, and mineral matter are all in close contact, and unavoidably all three components have a role to play during hydrocarbon generation and maturation reactions. Therefore, mineral matter catalytic effects and the interactions between the reactant phases (kerogen, bitumen and mineral matter all in intimate contact) should not be overlooked. In addition, water also play an important role during hydrocarbon generation and organic matter maturation as it is ubiquitous in sediments (Eglinton *et al*., 2006).

2.1 Fossil Fuels

A fossil fuel is a fuel formed by natural processes, such as anaerobic decomposition of buried dead organisms, containing energy originating in ancient photosynthesis. The adjective fossil means “obtained by digging: found buried in the Earth”. Such organisms and their resulting fossil fuels typically have an age of millions of years, and sometimes more than 650 million years. Fossil fuels contain high percentages of carbon and include petroleum, coal, and natural gas. Commonly used derivatives of fossil fuels include kerosene and propane. Fossil fuels range from volatile materials with low carbon-to-hydrogen ratios (like methane), to liquids (like petroleum), to nonvolatile materials composed of almost pure carbon, like anthracite coal. Methane can be found in hydrocarbon fields either alone or in association with oil (Carr *et al.,* 2009).

As of 2017 the world's primary energy sources consisted of petroleum (34 %), coal (28 %), natural gas (23 %), amounting to an 85 % share for fossil fuels in primary energy-consumption in the world. Non-fossil sources include nuclear (8.5 %), hydroelectric (6.3 %), and others (geothermal, solar, tidal, wind, wood, waste) amounting to 0.9 % (Arogundade and Ogunsuyi, 2021).

Although natural processes continually form fossil fuels, such fuels are generally classified as non-renewable resources because they take millions of years to form and the known viable reserves are being depleted much faster than new ones are being made. The use of fossil fuels also raises serious environmental concerns. The burning of fossil fuels produces around 21.3 billion tonnes of carbon dioxide (CO_2) per year (Behar *et al.,* 2007). It is estimated that natural processes can only absorb about half of that amount, so there is a net increase of 10.65 billion tonnes of atmospheric carbon dioxide per year. Carbon dioxide is a greenhouse gas that increases ‘radiative forcing’ and contributes to global warming. A global movement

towards the generation of low-carbon renewable energy is underway to help reduce global greenhouse-gas emissions. However, this study will focus on the alternative fuel from non-conventional source.

2.2 Coal

Coal is a combustible black or brownish-black sedimentary rock, formed as rock strata called coal seams. Coal is mostly carbon with variable amounts of other elements; chiefly hydrogen, sulfur, oxygen, and nitrogen. Coal is formed when dead plant matter decays into peat and is converted into coal by the heat and pressure of deep burial over millions of years. Vast deposits of coal originates in former wetlands called coal forests that covered much of the Earth's tropical land areas during the late Carboniferous (Pennsylvanian) and Permian times. As a fossil fuel burned for heat, coal supplies about a quarter of the world's primary energy and two-fifths of its electricity. Some iron and steel making and other industrial processes burn coal.

The extraction and use of coal causes many premature deaths and much illness. Coal industry damages the environment, including by climate change as it is the largest anthropogenic source of carbon dioxide, 14 Gt in 2016, which is 40 % of the total fossil fuel emissions. As part of the worldwide energy transition many countries have stopped using or use less coal, and the UN Secretary General has asked governments to stop building new coal plants by 2020. The largest consumer and importer of coal is China. China mines almost half the world's coal, followed by India with about a tenth. Australia accounts for about a third of world coal exports followed by Indonesia and Russia (Monthioux *et al.*, 2006).

2.3 Petroleum

Petroleum is a naturally occurring, yellowish-black liquid found in geological formations beneath the Earth's surface. Petroleum is formed when large quantities of dead organisms, mostly zooplankton and algae, are buried underneath sedimentary rock and subjected to both intense heat and pressure. It consists of naturally occurring hydrocarbons of various molecular weights and may contain miscellaneous organic compounds. It is commonly refined into various types of fuels. Components of petroleum are separated using fractional distillation; separation of a liquid mixture into fractions differing in boiling point using a fractionating column.

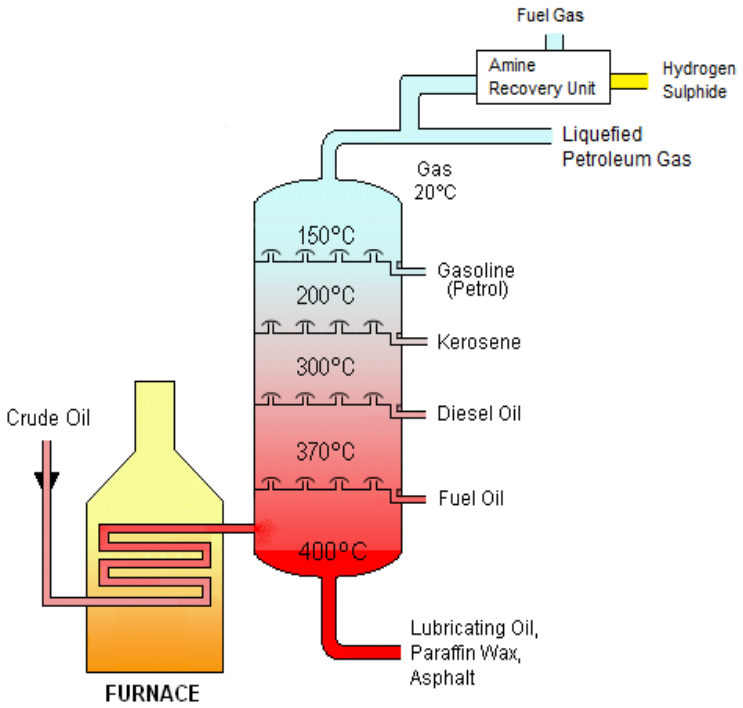

Figure 2.1: Petroleum refining process (Kelemen *et al*., 2014)

Petroleum has mostly been recovered by oil drilling. Drilling is carried out after studies of structural geology (at the reservoir scale), sedimentary basin analysis, and reservoir

characterization (mainly in terms of the porosity and permeability of geologic reservoir structures) are been completed. Petroleum is refined and separated, most easily by distillation, into numerous consumer products, from gasoline (petrol) and kerosene to asphalt and chemical reagents used to make plastics, pesticides and pharmaceuticals. Petroleum is used in manufacturing a wide variety of materials, and it is estimated that the world consumes about 95 million barrels each day (Mitra-Kirtley *et al.,* 2016).

Crude oil extracted from geological sources is a mixture of a wide range of hydrocarbons starting from lightest methane to heavy long chain hydrocarbons found in tar. The hydrocarbons are often accompanied by water, H_2S, particulate matter such as sand etc. This crude oil stream undergoes an elaborate refining process which comprises of separation of different cuts of hydrocarbons, conversion of some hydrocarbons into more desirable products and purification of extra substances such as sulphur before shipping it away (Speight, 2009). As shown in Figure 2.1 above, the lightest gas (C1 to C3), called fuel gas are separated at atmospheric pressure from rest of the crude oil and is used in the refinery as fuel gas. This is not an end-product of the refining process, as the excess fuel gas is flared off. Fuel gas is used for various purposes in the refinery including blanketing gas. Liquefied Petroleum Gas, LPG is mainly mixture of propane and butane (C3+C4). These gases separated from the top of Atmospheric Distillation Unit (or Crude Distillation Unit - CDU) are liquefied under pressure and sold as cooking fuel. Petrol or Gasoline is one of the commonly used automotive fuels. It is a mixture of cyclic compounds known as ‘napthas’. Most of refinery produced kerosene can be used as high quality Aviation Turbine Fuel (ATF). Some of that kerosene can be used for domestic purposes as heating / cooking oil. Kerosene is less volatile than gasoline and separated from crude oil after the napthas have boiled off. Diesel oil is primarily used as transportation fuel in compression ignition engines

in various types of vehicles. A kind of diesel oil also known as ‘gas oil’ can be domestically used for heating. Diesel is less volatile (or heavier) than gasoline and kerosene. A range of different grades of fuel oils are produced from crude oil after boiling off the lighter products such as gasoline, naptha, kerosene etc. The lighter grades of fuel oil are used as transportation fuel for compression engines with low velocities and heavier grades of fuel oil are used as fuel to boilers, power stations etc. This is the heaviest cut of hydrocarbons left at the bottom after boiling off all the hydrocarbons usable as fuels. It is primarily used as road covering material, but can also be used as a waterproofing material. Crude oil production is generally accompanied by H_2S gas. This H_2S gas is separated from rest of the crude oil along with fuel gas - methane and ethane (C1 & C2). H_2S is separated from the fuel gas in Amine Recovery Unit (ARU) and further, pure sulphur is separated in the Sulphur Recovery Unit (SRU). This sulphur in liquefied form is sold to the fertilizer manufacturers (Kelemen *et al*., 2014**).**

The use of petroleum as fuel is controversial due to its impact on global warming and ocean acidification. According to the UN's Intergovernmental Panel on Climate Change, fossil fuel phase-out, including petroleum, needs to be completed by the end of 21st century to avoid "severe, pervasive, and irreversible impacts for people and ecosystems" (Mitra-Kirtley *et al.*, 2016).

2.4 Gas

Natural gas is a naturally occurring hydrocarbon gas mixture consisting primarily of methane, but commonly including varying amounts of other higher alkanes, and sometimes a small percentage of carbon dioxide, nitrogen, hydrogen sulfide, or helium. Natural gas is a non-renewable hydrocarbon used as a source of energy for heating, cooking, and electricity generation. It is also used as a fuel for vehicles and as a chemical feedstock in the manufacture of plastics and other commercially important organic chemicals. It is formed when layers of

decomposing plant and animal matter are exposed to intense heat and pressure under the surface of the Earth over millions of years. The energy that the plants originally obtained from the sun is stored in the form of chemical bonds in the gas.

Natural gas is found in deep underground rock formations or associated with other hydrocarbon reservoirs in coal beds and as methane clathrates. Most natural gas was created over time by two mechanisms: biogenic and thermogenic. Biogenic gas is created by methanogenic organisms in marshes, bogs, landfills, and shallow sediments. Deeper in the earth, at greater temperature and pressure, thermogenic gas is created from buried organic material. In petroleum production, gas is sometimes burned as flare gas. Before natural gas can be used as a fuel, most, but not all, must be processed to remove impurities, including water, to meet the specifications of marketable natural gas. The by-products of this processing include: ethane, propane, butanes, pentanes, and higher molecular weight hydrocarbons, hydrogen sulfide (which may be converted into pure sulfur), carbon dioxide, water vapor, and sometimes helium and nitrogen (Michels *et al.,* 2005).

2.4.1 Hubbert peak theory

The Hubbert peak theory says that for any given geographical area, from an individual oil-producing region to the planet as a whole, the rate of petroleum production tends to follow a bell-shaped curve. It is one of the primary theories on peak oil. The Hubbert peak theory is based on the observation that the amount of oil under the ground in any region is finite; therefore the rate of discovery which initially increases quickly must reach a maximum and decline. In the US, oil extraction followed the discovery curve after a time lag of 32 to 35 years (Meredith *et al.,* 2012). The theory is named after American geophysicist Dr. Marrion King Hubbert, who created a method of modeling the production curve given an assumed ultimate recovery volume.

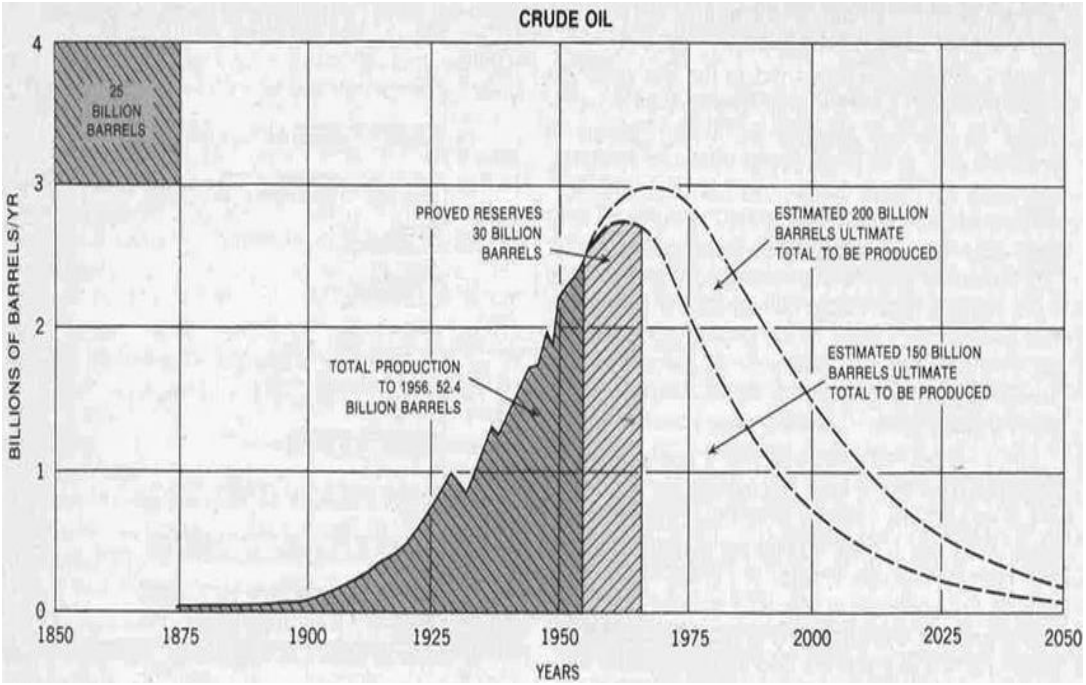

Figure 2.2: Depiction Hubbert's Peak Theory (Pomerantz *et al*., 2013)

Choosing a particular curve determines a point of maximum production based on discovery rates, production rates and cumulative production. Early in the curve (pre-peak), the production rate increases due to the discovery rate and the addition of infrastructure. Late in the curve (post-peak), production declines because of resource depletion.

2.5 Unconventional Crude Oil

Unconventional oil is petroleum produced or extracted using techniques other than the conventional (oil well) method. Oil industries and governments across the globe are investing in unconventional oil sources due to the increasing scarcity of conventional oil reserves. Unconventional oil sources include oil sands, oil shale and heavy oil (Stainforth, 2009).

2.5.1 Oil shale

Oil shale is an organic-rich fine-grained sedimentary rock containing kerogen (a solid mixture of organic chemical compounds) from which liquid hydrocarbons can be produced,

called shale oil (not to be confused with tight oil—crude oil occurring naturally in shales). Shale oil is a substitute for conventional crude oil; however, extracting shale oil from oil shale is more costly than the production of conventional crude oil both financially and in terms of its environmental impact (Van Graas *et al.*, 2001). Heating oil shale to a sufficiently high temperature causes the chemical process of pyrolysis to yield a vapor. Upon cooling the vapor, the liquid shale oil is separated from combustible oil-shale gas (the term *shale gas* can also refer to gas occurring naturally in shales). The general composition of oil shales constitutes inorganic matrix, bitumen and kerogen. Oil shales differ from oil-*bearing* shales, shale deposits that contain petroleum (tight oil) that is sometimes produced from drilled wells. Examples of oil-*bearing* shales are the Bakken Formation, Pierre Shale, Niobrara Formation, and Eagle Ford Formation (Knauss *et al.*, 2007).

2.5.2 Heavy oil

Heavy crude oil is closely related to natural bitumen from oil sands. Petroleum geologists categorize bitumen from oil sands as 'extra-heavy oil' due to its density of less than 10 °API. Bitumen is the heaviest, thickest form of petroleum. Natural bitumen, also called tar sands or oil sands, shares the attributes of heavy oil but is yet more dense and viscous. Natural bitumen (often called tar sand or oil sand) and heavy oil differ from light oils by their high viscosity (resistance to flow) at reservoir temperatures, high density (low API gravity), and significant contents of nitrogen, oxygen, and sulfur compounds and heavy-metal contaminants (Hart, 2012).

Controlling the H/C ratio of the products would require either lowering the C content of the products (carbon rejection), or increasing the H content (hydrogen addition). Figure 2.3 depicts the two major paths for upgrading heavy oil.

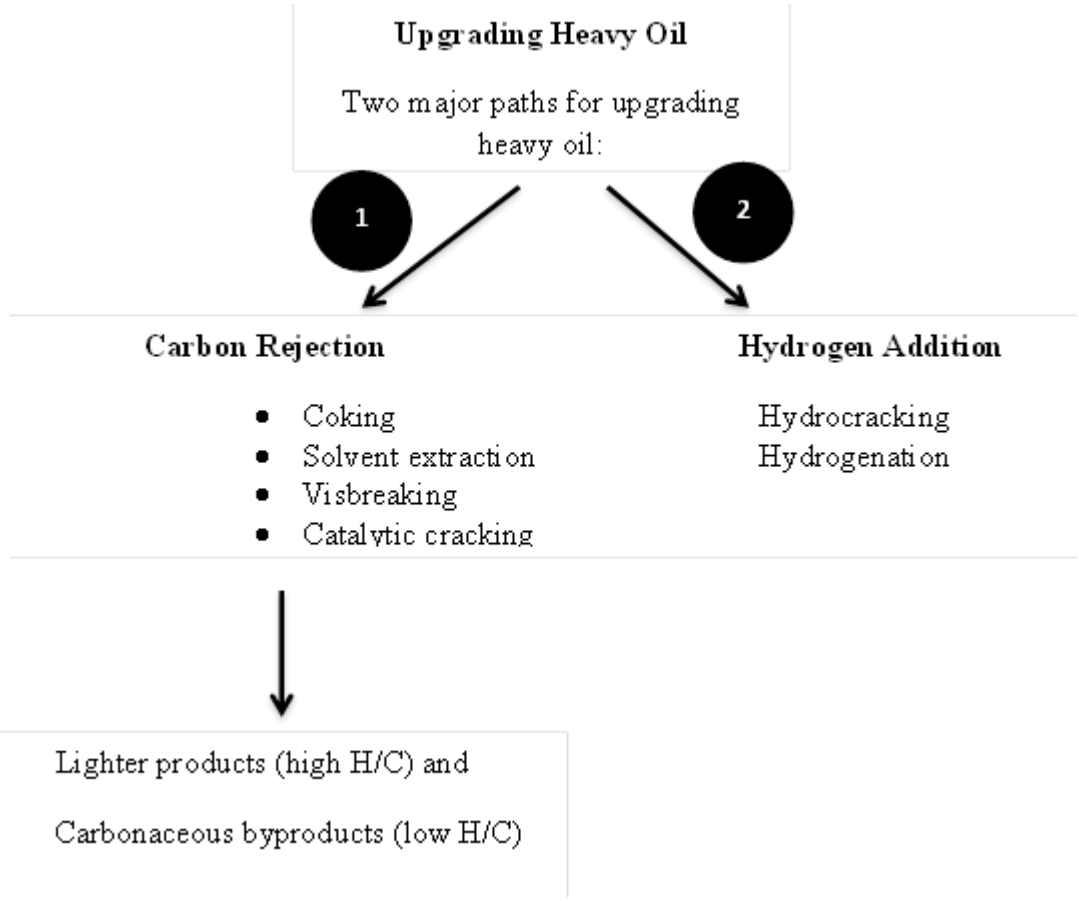

Figure 2.3: Processes of upgrading heavy oil (Hart, 2012)

The processes, coking, solvent extraction (deasphalting), visbreaking, and catalytic cracking reject carbon in the coke (carbonaceous) product so that lighter products (with high H/C) ratios can be obtained in these processes. In contrast, hydrogen addition, as in the processes of hydrogenation and hydrocracking, enables the conversion of all the carbon present in heavy oil to high value products without rejecting, or sacrificing. One might ask, then, why would any refinery carry out any carbon rejection process instead of hydrogen addition? A short answer to this question is that the hydrogen addition processes cost much more than carbon rejection processes, because producing hydrogen and the catalysts used in hydrogen addition processes are very expensive.

Similarly, to transport heavy oils more economically, the pressure drop in the pipeline must be lowered to minimize the pump power required to push the oil over a long distance. However, because of their high viscosity, conventional pipelining is not adequate for transporting heavy oils and bitumen to refineries without reducing their viscosity (Hart, 2012). As shown in Figure 2.4, the methods used for transporting heavy oil and bitumen through pipelines are generally grouped into three: viscosity reduction [preheating of the heavy oil and bitumen and subsequent heating of the pipeline, blending and dilution with light hydrocarbons or solvent, emulsification through the formation of an oil-in-water emulsion and lowering the oil's pour point by using pour point depressant (PPD)]; drag/friction reduction (pipeline lubrication through the use of core-annular flow, drag-reducing additive); and In-Situ upgrading of the heavy oil to produce a synthetic crude oil with improved viscosity, American Petroleum Institute (API) gravity, and minimized asphaltenes, sulphur and heavy metal content (Pomerantz *et al*., 2013).

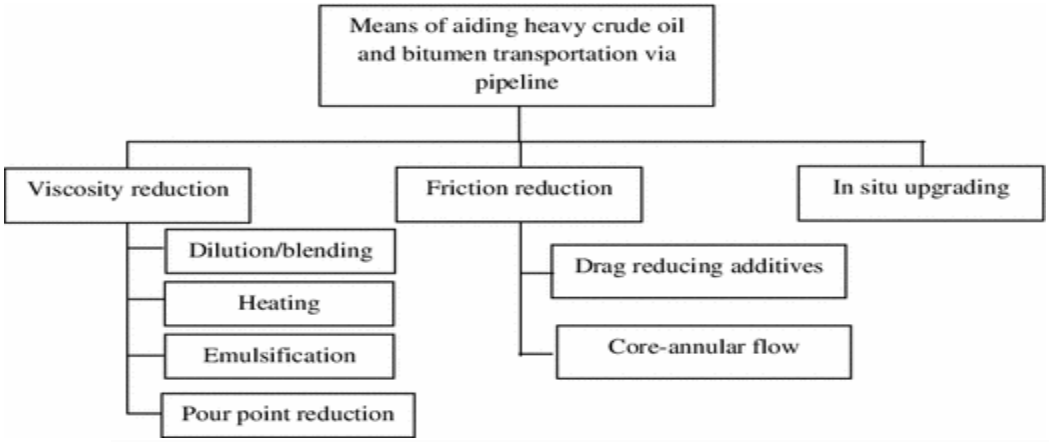

Figure 2.4: Diagrammatic display of methods of improving heavy crude oil and bitumen flow via pipelines (Pomerantz *et al*., 2013)

In the past, heavy crude oil and bitumen production was considered to be uneconomic, because of the intensive cost of recovery, transportation, refining and low market value. Additionally, the decline of conventional middle and light crude oil as well as the ever-

growing world energy demand drives the exploitation of this hydrocarbon resource. In Canada, about 700,000 barrels per day of synthetic crude oil is obtained from bitumen (tar sands) and is transported via pipelines to refineries in Canada and the USA (Kelemen *et al*., 2010).

2.5.3 Oil sand

Oil sands or more technically bituminous sands are a type of unconventional petroleum deposit. Oil sands are either loose sands or partially consolidated sandstone containing a naturally occurring mixture of sand, clay, and water, saturated with a dense and extremely viscous form of petroleum technically referred to as bitumen (or colloquially as tar due to its superficially similar appearance). Natural bitumen deposits are reported in many countries and are found in extremely large quantities in Canada. Other large reserves are located in Kazakhstan, Russia, and Venezuela. The estimated worldwide deposits of oil are more than 2 trillion barrels (320 billion cubic metres), the estimates include deposits that have not been discovered. Proven reserves of bitumen contain approximately 100 billion barrels, and total natural bitumen reserves are estimated at 249.67 Gbbl (40 billion cubic metres) worldwide (Price and Wenger, 2012).

2.6 Kerogen

Kerogen is termed as the insoluble macromolecular material comprising mixtures of macerals and reconstituted degradation products of organic matter (Durand, 2003). With increased burial depth and subsequent temperature increase, the thermodynamically unstable kerogen is decomposed and transformed by means of a complex network of reactions into increasingly more stable compounds (Hoering, 2004). Kerogens typically contain carbon, hydrogen and oxygen elements. The composition of the kerogen is dependent on the initial input of organic matter and the nature and extent of microbial activity in the upper

sedimentary layers during diagenesis. Consequently, they can be classified into four types namely; Type I, Type II, Type III and Type IV (or residual kerogen) (Tissot and Welte, 2004). Type I kerogen is proposed to be derived from algal lipids (fresh water alga botryococcus braunii) or organic matter enriched in lipids via microbial activity. It is formed in relatively fine-grained, organic-rich, and anoxic muds that are deposited in quiet, oxygen-deficient, shallow water environments such as lagoons and lakes (Speight, 2009). Type II kerogen is usually derived from mixtures of phytoplankton, zooplankton and micro-organisms that were deposited in a reducing environment. It contains a significant amount of polyaromatic nuclei, heteroaromatic ketones, carboxylic acid groups and ester bonds (Tissot and Welte, 2004; Speight, 2009). Type III kerogens are derived from woody terrestrial material consisting of a few long chains (≥ C25) originating from higher plant waxes (lipinites), cutin (exinites), and some chains of medium length (C15 to C20) from vegetable fats, methyl groups and other short chains (Mcnab *et al.,* 2002). Type IV kerogen (residual kerogen) primarily comprises a black opaque debris largely composed of carbon in the form of inertinite and abundant aromatic nuclei and oxygen containing groups in the absence of aliphatic chains. It exhibits a very low H/C ratio (< 0.8) and a high O/C ratio and is incapable of generating hydrocarbons. It is considered as a form of "dead carbon" in the sense of petroleum generation; however they have also been regarded principally as gas producers with much less oil potential than type I to type III kerogens (Speight, 2009).

2.7 Bitumen

Bitumen consists of solid or liquid hydrocarbons and other organic compounds that can be extracted from fine-grained sedimentary rocks using organic solvents such as carbon disulphide or dichloromethane (Carr *et al*., 2009). It comprises four main fractions namely;

asphaltenes, resins, saturates and aromatics. Asphaltenes and resins are heavy N, S, O containing molecule and are the higher molecular polycyclic fractions constituents of bitumen and crude oils (Czarnecka and Gillott, 2000). Resins and asphaltenes are usually distinguished by their separation procedures (Greenfield *et al.,* 2015). Asphaltenes precipitate from crude oil when a large quantity of low-molecular weight alkanes is added (such as *n*-pentane), while resins (polars) remain in solution. Both resins and asphaltenes comprises around 0-40 % of non-degraded crude oils, depending on genetic type and thermal maturity. They are usually in high concentration in shallow immature petroleum and decreases with increasing depth and subsequent cracking (25-60 %) due to microbial activity, water washing and oxidation (Ogundele *et al.,* 2019) suggested that bitumen is formed during the diagenesis stage at the expense of kerogen, where the heteroatomic bonds are broken successively. The formation of bitumen is an intermediate to kerogen decomposition and oil generation involving the breaking of weak bonds within the kerogen (Freund *et al.*, 2003). Bitumen is frequently found filling pores and crevices of sandstone, limestone or argillaceous sediments, in which case the organic and associated mineral matrix is known as rock asphalt (Evans *et al.,* 2001).

2.7.1 Bitumen in Nigeria

Bitumen is one of the richly deposited mineral resources in Nigeria just like crude oil, it is found in Ondo, Lagos, Ogun, and Edo State. Bitumen was discovered first in the 1900s, with exploration beginning in 1905. A technical and economic evaluation of Bitumen in Nigeria was conducted and it was observed that it contain oil with an estimate of more than 13 to 14 billion barrels of oil (Onojake and Ndubuka, 2016).

Bitumen also referred to as Asphalt is a sticky, black and highly viscous liquid or semi-solid form of petroleum. It may be found in natural deposits or may be a refined product; it is a substance classed as a pitch. The estimated probable reserve of bitumen in Ondo State is about 16 billion barrels (Uguna *et al*., 2012).

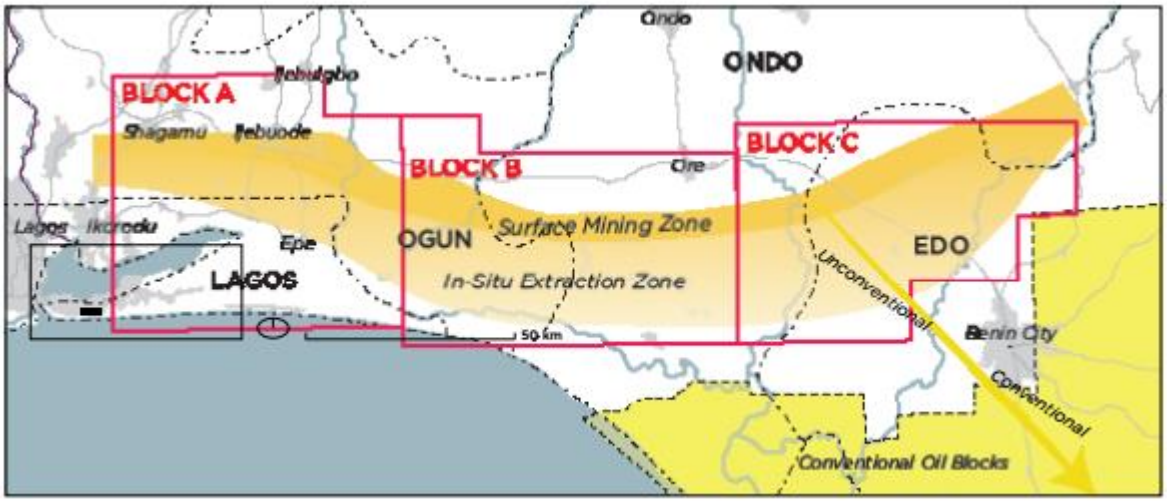

Figure 2.5: Bitumen Deposits in Nigeria (Ojeyemi *et al*., 2015)

Nigeria has one of the largest deposits of bitumen in the world, spanning approximately 120km. The primary use (70%) of bitumen is in road construction, where it is used as the glue or binder mixed with aggregate particles to create asphalt concrete. Its other main uses are for bituminous waterproofing products, including production of roofing felt and for sealing flat roofs (Ojeyemi *et al*., 2015).

In as much as the mineral resources can richly serve as an alternative to crude oil which has decline over the years, it is good to know also about the implications involved in the mining as it can lead to deforestation and likely affect most Local Government Areas of Ondo State, where the bitumen deposit is in huge quantity and recorded as the largest deposit in Africa (Kelemen *et al.*, 2014).

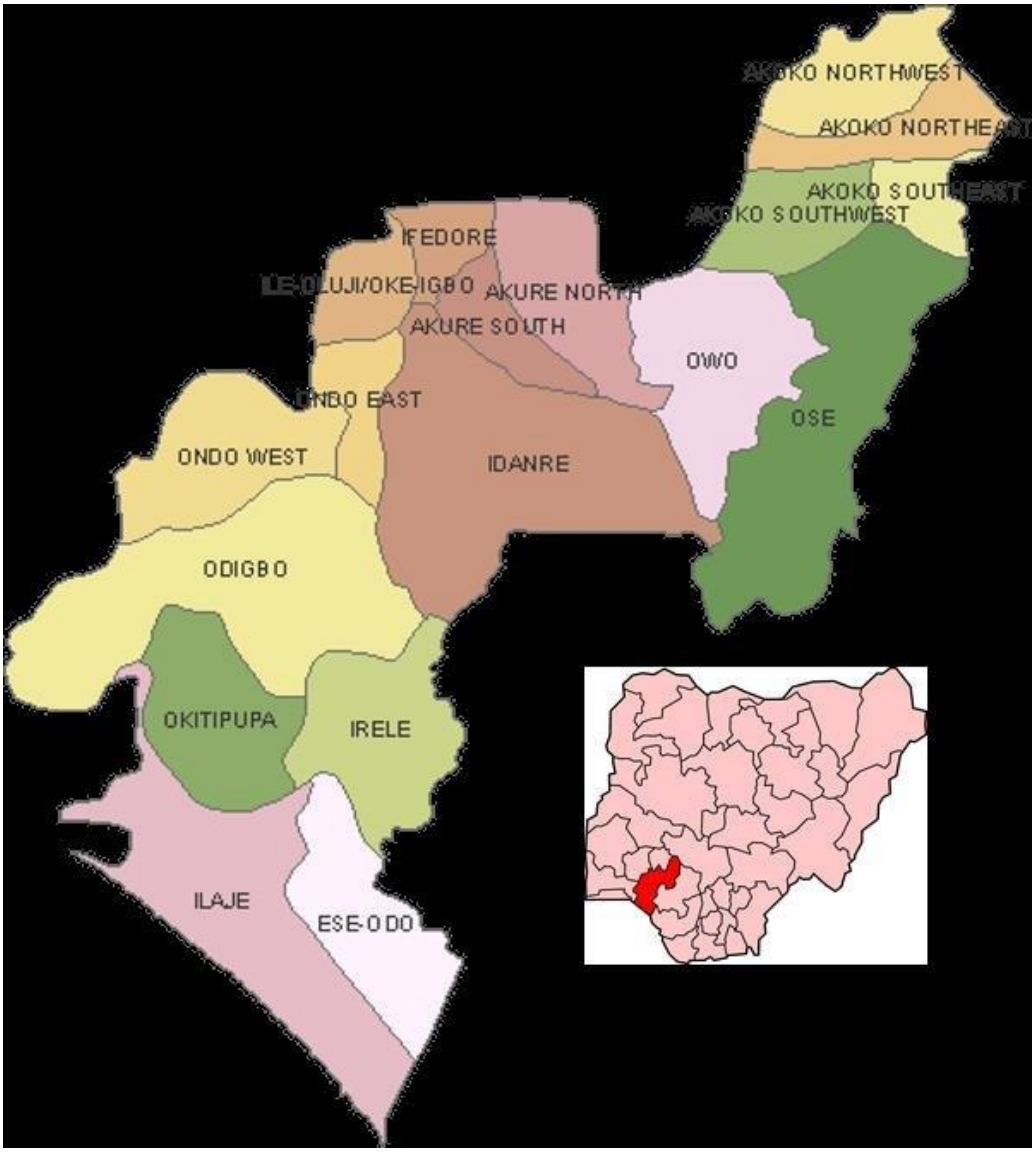

Figure 2.6: Map of Ondo State showing the eighteen local government areas (Uguna *et al*., 2012)

2.7.2 Bitumen extraction

There are two broad techniques of bitumen extraction used: surface mining and in-situ. The method used depends on the depth of the reservoir. Deposits located at a depth of less than 75 meters can technically be surface mined, although most deposits are located at a depth of less than 50 meters. In Nigeria, bitumen typically occurs both on the surface and sub-surface (Shedrach *et al.,* 2018).

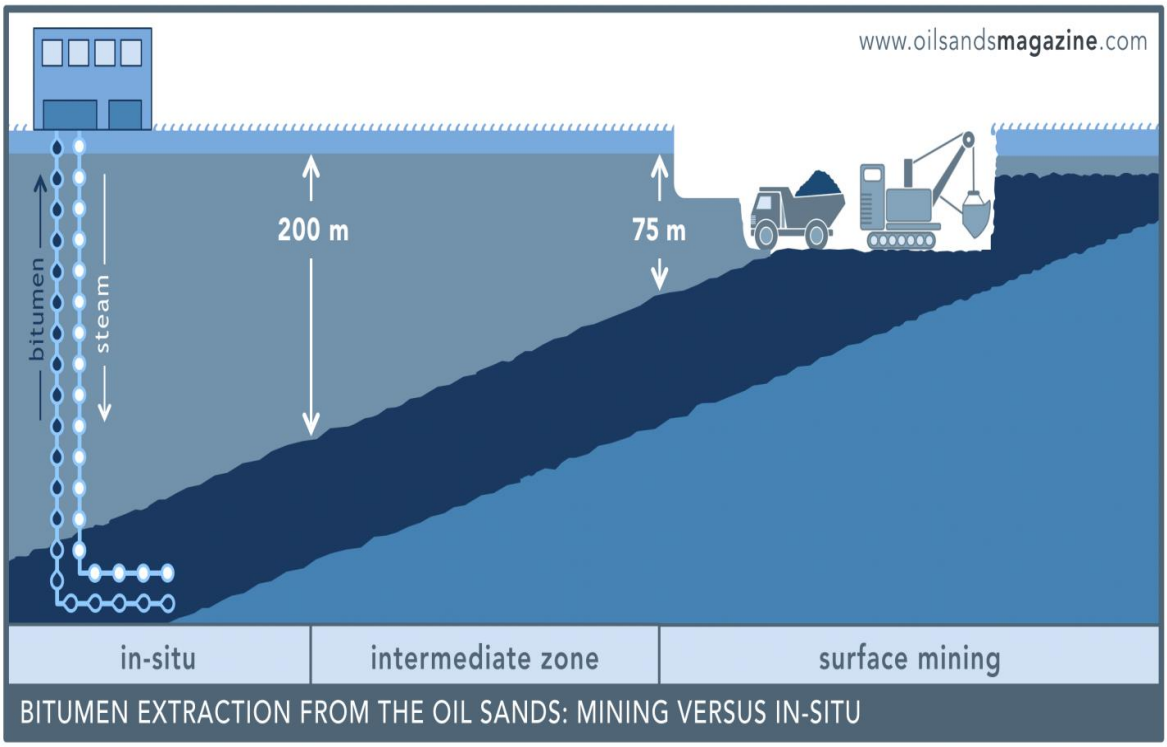

Figure 2.7: Bitumen Extraction (Meredith *et al*., 2012)

The bitumen recovery process is slightly different for mining versus in-situ facilities. Mined oil sands requires large amounts of process water to separate the bitumen from the sand, while the in-situ process requires less water but greater volumes of steam. In both cases, the resulting bitumen product can either be sent to an Upgrader for conversion to synthetic crude oil or diluted and sold directly to refineries (Shedrach *et al.,* 2018).

The three potential methods of bitumen extraction in Nigeria are:

(a) Small-Scale surface mining

(b) Large-Scale surface mining

(c) Thermal (In-situ) extraction method

2.8 Pyrolysis

Pyrolysis process is the thermal decomposition of a material at elevated temperature in an inert atmosphere. It involves a change of chemical composition. The word is coined from the Greek words *pyro* "fire" and *lysis* "separating". Pyrolysis techniques can be used in laboratories to simulate and study organic matter evolution occurring in the sedimentary basins and replicating it on a human time scale. Pyrolysis is the decomposition of organic matter through thermal energy (Wampler, 2007). Furthermore, by studying the resulting yields, we are able to understand more on the evolution of organic matter in the sedimentary basins (Peters *et al.*, 2000).

There are various types of pyrolysis techniques used such as confined and unconfined pyrolysis, flash pyrolysis and hydropyrolysis, to name a few. In confined pyrolysis, samples are heated in gold tubes or gold cells, where the pressurizing medium is usually not in contact with the samples (Michels *et al*., 2004). For unconfined pyrolysis conditions, the samples are in contact with the pressurizing medium which is usually heated in autoclave vessels (Lewan *et al*., 2018). Experiments using the confined or unconfined techniques can either be heated without water (anhydrous pyrolysis) (Carr *et al*., 2009); with varying amounts of water (hydrous pyrolysis or high water pressure pyrolysis) (Michels *et al*., 2005).

2.8.1 Anhydrous pyrolysis

Anhydrous pyrolysis is where the samples are heated in the absence of water either in an open or closed system (Carr *et al*., 2009; Knauss *et al*., 2007). The Rock Eval pyrolysis is an example of an open anhydrous system where the samples are heated in an inert atmosphere in which a carrier gas is passed over the heated sample. The pyrolysis product is allowed to escape from the sample where it is then swept by the carrier gas and quantified by an FID, or swept through a cold trap to be quantified by GC analysis (Meredith *et al*., 2012). Another example of an open anhydrous system is hydropyrolysis where samples heated with different heating rates under high hydrogen gas pressure (> 10 MPa) (Berwick *et al*., 2017).

In a closed system, the samples are heated under an inert atmosphere in a sealed reactor such as gold cells or tubes, silica glass tubes, mini-autoclave/tubes or reaction vessels (Carr *et al*., 2009). In this case, the pyrolysate are extracted at the end of the experiment. Other forms of pyrolysis are methane pyrolysis, dry distillation, destructive distillation, caramelization, high-temperature cooking processes, thermal depolymerization, ceramization, flash vacuum pyrolysis and cracking of heavier hydrocarbons into lighter ones, as in oil refining. Cracking is the process whereby complex organic molecules such as kerogens or long-chain hydrocarbons are broken down into simpler molecules by the breaking of carbon-carbon bonds in the precursors. The rate of cracking and the end products are strongly dependent on the temperature and presence of catalysts. Thermal cracking is currently used to "upgrade" very heavy fractions or to produce light fractions or distillates, burner fuel and petroleum coke. The catalytic cracking process involves the presence of acid catalysts, usually silica-alumina and zeolites. The catalysts promote the formation of carbocations, which undergo processes of rearrangement and scission of C-C bonds. Relative to thermal cracking, catalytic cracking proceeds at milder temperatures and saves energy.

2.8.2 Hydrous pyrolysis

Hydrous pyrolysis is a hydrothermal experiment which involves the heating of samples in a closed vessel in the presence of water (Lewan *et al*., 2018). This method of pyrolysis usually requires the heated samples to be in contact with or submerged in liquid water, not water vapour or supercritical fluid. When using whole rock samples the presence of water appears to recreate more closely the conditions of naturally occurring environments. Hydrous pyrolysis conducted by Lewan, shows that heating organic-rich rocks at 330 °C for 72 hours in the presence of liquid water resulted in the generation and expulsion of a petroleum like oil that are absent in olefins, similar to natural crude oils.

The generation of petroleum can be classified into four distinct stages namely, pre-oil generation, incipient oil generation, primary oil generation and post-oil generation (Lewan *et al*., 2018).

Hydrous pyrolysis studies on source rocks has provided information on stages, kinetics and thermal maturation indices of petroleum formation (Lewan, 2002), revealing complete biomarker potential and transformations of a source rock, maturation of organic carbon isotopes, primary migration and expulsion of oil, oil generation from coals and increasing carbon dioxide gas and total extractable bitumen and oil, (Carr *et al*., 2009) compared to anhydrous pyrolysis. These authors all came to a similar conclusion that experiments performed under hydrous conditions may provide a more realistic simulation of organic matter transformations present in the sedimentary basins (Eglinton *et al.*, 2006).

2.9 Equipment for Hydrous Pyrolysis

2.9.1 Autoclave

An autoclave is a pressure chamber used to carry out industrial and scientific processes requiring elevated temperature and pressure different from ambient air pressure. Many autoclaves are used to sterilize equipment and supplies by subjecting them to pressurized saturated steam at 121 °C (249 °F) for around 15-20 minutes depending on the size of the load and the contents. Generally, Autoclaves are used in medical applications to perform sterilization and in the chemical industry to cure coatings and vulcanize rubber and for hydrothermal synthesis. The name comes from Greek *auto-*, ultimately meaning self, and Latin *clavis* meaning key, thus a self-locking device. Sterilization autoclaves are widely used in microbiology, medicine, podiatry, tattooing, body piercing, veterinary medicine, mycology, funerary practice, dentistry, and prosthetics fabrication. They vary in size and function depending on the media to be sterilized and are sometimes called retort in the chemical and food industries (Lewan *et al*., 2018).

Figure 2.8: Illustration of an Autoclave (Lewan *et al*., 2018)

2.9.2 Horizontal tubular furnace

The 1200 ^{o}C tube furnace is a precision bench-top furnace using resistance wire as heating elements. It is widely used for materials or chemical lab to sinter all types of new material samples under vacuum. It is controlled by high precision SCR (Silicon Controlled Rectifier) digital controller with accuracy +/-1C and 30 segments programmable up to 1200 ^{o}C. It has a maximum temperature of 1200 ^{o}C and a maximum heating rate of 30 ^{o}C /min. The furnace body is sometimes detachable from the control box to allow use of optional mounting arrangements and the wire elements which are alloy of Iron, Chromium and Aluminum, in high quality vacuum insulation ensure fast heat up and excellent temperature uniformity (Pomerantz *et al.*, 2013).

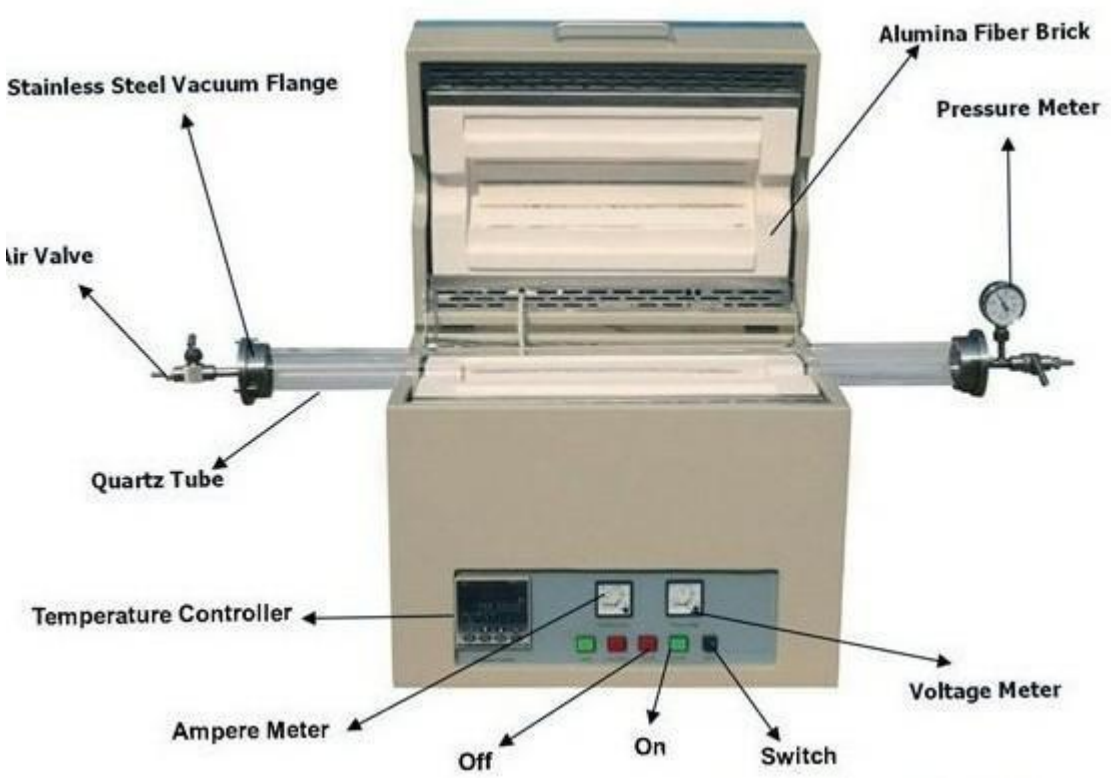

Figure 2.9: 1200-Degree lab-scale Nitrogen atmosphere horizontal tubular furnace (Pomerantz *et al.*, 2013).

2.10 Study of Kinetics

Chemical reaction kinetics is a branch of Chemical Engineering that is concerned with understanding the rates of chemical reactions. It includes investigations of how experimental conditions influence the speed of a chemical reaction and yield information about the reaction's mechanism and transition states, as well as the construction of mathematical models that also can describe the characteristics of a chemical reaction. The factors that affect rates of reaction are nature of the reactants, surface area of solid state, concentration, temperature, pressure and presence of catalyst. The reaction rate varies depending upon what substances are reacting. The nature and strength of bonds in reactant molecules greatly influence the rate of their transformation into products (Shabbar *et al*., 2018).

High temperature devolatization plays an important role in the pyrolysis of bitumen. Therefore it is necessary to develop models to predict the behavior of the feedstock when it is subjected to high temperature. The relationship between the extents of reaction as it proceeds with the temperature can be determined by Arrhenius equation. Activation energy (E) and pre-exponential factor (A) are the two important parameters in Arrhenius equation which are determined by thermal analysis. Thermogravimetric analysis (TGA) is extensively used to determine the global kinetic parameters of pyrolysis and combustion. There are various models to analysis of non-isothermal solid-state kinetic data from TGA. These models can be categorized under two main headings: model fitting and model-free (isoconversional). Model fitting approach is incapable of determining the reaction model uniquely and, therefore, it becomes difficult to reach a reliable mechanistic conclusion. On the other hand, model-free methods allow the dependence of activation energy on the extent of conversion, which in turn provides a reliable reaction rate prediction so that a mechanistic conclusion could be drawn. The terms 'model-free' and 'isoconversional' are sometimes used interchangeably, but not all model-free methods are isoconversional, Kissinger method is one of these exceptions. Coats-Redfern use data from thermogravimetric analysis to evaluate kinetic parameters at constant heating rate (Azharul *et al*., 2016). Equation 2.1 shows the Coats-Redfern equation.

$$In\left(\frac{g(\alpha)}{T^2}\right) = In\left(\frac{AR}{\beta E}\right) - \frac{E_a}{RT} \qquad (2.1)$$

CHAPTER THREE

3.0 MATERIALS AND METHODS

3.1 Material

The bitumen sample was collected from Agbabu community in Odigbo local government area of Ondo State and was preserved in a sealed container.

3.2 Equipment

The list of equipment used for experiment and analyses are shown in Table 3.1.

Table 3.1: List of experimental and analytical equipment

Experimental and Analytical Equipment	Model
Viscometer	Saybolt Furol PT-82F
Digital Density meter	Anton Paar DMA-5
Flash Point Apparatus	C-TECH SYD-3536
Horizontal Tubular Furnace	STG-100-12
Weighing balance	Scout Pro SP401
TGA	PerkinEimer TGA-4000
SEM	PHENOM ProX
FT-IR	Shimadzu IRAffinity-1S
GCMS	Agilent 5973-MSD
XRF	Philip PW 1210

3.3 Characterization of the Bitumen

3.3.1 Thermogravimetric analysis

The TGA was carried out on a thermogravimetric analyzer (Plate I) which continually measured the mass of the bitumen as the temperature is changed over time. The TGA is done at a heating rate of 10 ^{o}C /min in inert environment.

Plate I: TGA determination setup (FUT Minna, Step B)

3.3.2 Scanning electron microscopy

The surface and microstructure analysis of the bitumen sample was carried out using a SEM instrument model PHENOM ProX, Phenom World Einhoven, The Netherlands (Plate II). The sample was mounted onto the SEM stubs (layered with sticky carbon tape). The stub was then placed in a sputter coater (Quorum Technologies model Q150R) for five minutes for coating with 5nm of gold to provide high reflectivity during the scanning process. The sample was placed at 40 °C in an oven before SEM images and EDX results of the sample were generated. Thereafter the sample was taken to the SEM equipment where it was viewed via NaVCaM for focusing and resolution adjustment for the focus and brightness, afterward the morphologies at particular magnification was taken and recorded (Shedrach *et al.*, 2018).

Plate II: SEM analysis equipment (Shedrach *et al.*, 2018)

3.3.3 Fourier transform infrared (FTIR)

For the FT-IR the Shimadzu Fourier Transform Infrared Spectrophotometer-FTIR 8400S (PLATE III) equipped with Win-IR Pro software was used. The following settings are used: background scans 10; sensitivity 2.0; wavelength range 500-4000 cm^{-1}, and 4 cm^{-1} scan resolution. The bitumen sample was dissolved in chloroform up to 30 mg/ml concentration, the solution was allowed to sit for 1 hour for thorough dissolution to take place before it was pipetted and dropped unto the Potassium Bromide, KBr crystal to form a uniform thickness. The crystal was dried with a stream of nitrogen gas and allowed to sit for 20 minutes to dry properly. The crystal was then placed in the FT-IR chamber for scanning (Arogundade and Ogunsuyi, 2021).

Plate III: FT-IR analysis equipment (Arogundade and Ogunsuyi, 2021)

3.3.4 Gas chromatography mass spectrometry (GC-MS)

The composition of the bitumen sample and the yields from hydrous and anhydrous pyrolysis were analyzed using gas chromatography and mass spectrometry (GCMS) instrument (GC/MS-QP2010-Ultra) (PLATE VII), equipped with flame ionization and mass spectrometry detection. The pretreatment involves dissolving the samples into n-heptane in order to separate the dissolvable maltenes (saturates, aromatics and resins) from the non-dissolvable asphaltene, this is schematically shown in the diagram below. A capillary column coated with a 0.25 um film of DB-5 with length of 30 m and diameter 0.25 mm was used. The gas spectrometer is equipped with a split injector at 200 ^{o}C and has a split ratio of 1:10. Helium gas of 99.95 % purity was used as carrier gas at flow rate of 1.51 ml/min. The oven initial temperature was set to 70 ^{o}C for 2 min and then increased to 300 ^{o}C at a rate of 10 ^{o}C/minute for 7 minutes. All the compounds were identified by means of the NIST library. The mass spectrometer was operated at an interface temperature of 240 ^{o}C with ion source temperature of 200 ^{o}C of range 40 – 1000 m/z (Ogundele *et al.,* 2019).

3.4 Determination of Physicochemical Properties

Experiments were carried out on the bitumen to determine its physicochemical properties, the properties determined include: viscosity, density, specific gravity and flash point. The Saybolt Furol Viscometer (Plate IV) was used to determine the kinematic viscosity of the bitumen. The experimental setup includes Saybolt Furol viscometer, two thermometers, stopwatch and water bath (Ojeyemi *et al.,* 2015), while the flash point of the bitumen was determined with the 'open cup' test apparatus (Plate VI). Density of the Bitumen is determined using Anton-Paar digital density meter (Plate V) and the specific gravity is determined by the use of a 10ml beaker. The API gravity is determined from equation 3.1. The results are as reported in Chapter 4 below.

From the relation for API and specific gravity (Shedrach *et al.,* 2018),

$$\text{API} = \frac{141.5}{Specific\ Gravity} - 131.5 \qquad (3.1)$$

Plate IV: Saybolt Furol Viscometer (Uguna *et al.,* 2012)

Plate V: Anton Paar digital density meter (Pan *et al.*, 2012)

Plate VI: Flash Point determination apparatus (Ojeyemi *et al.*, 2015)

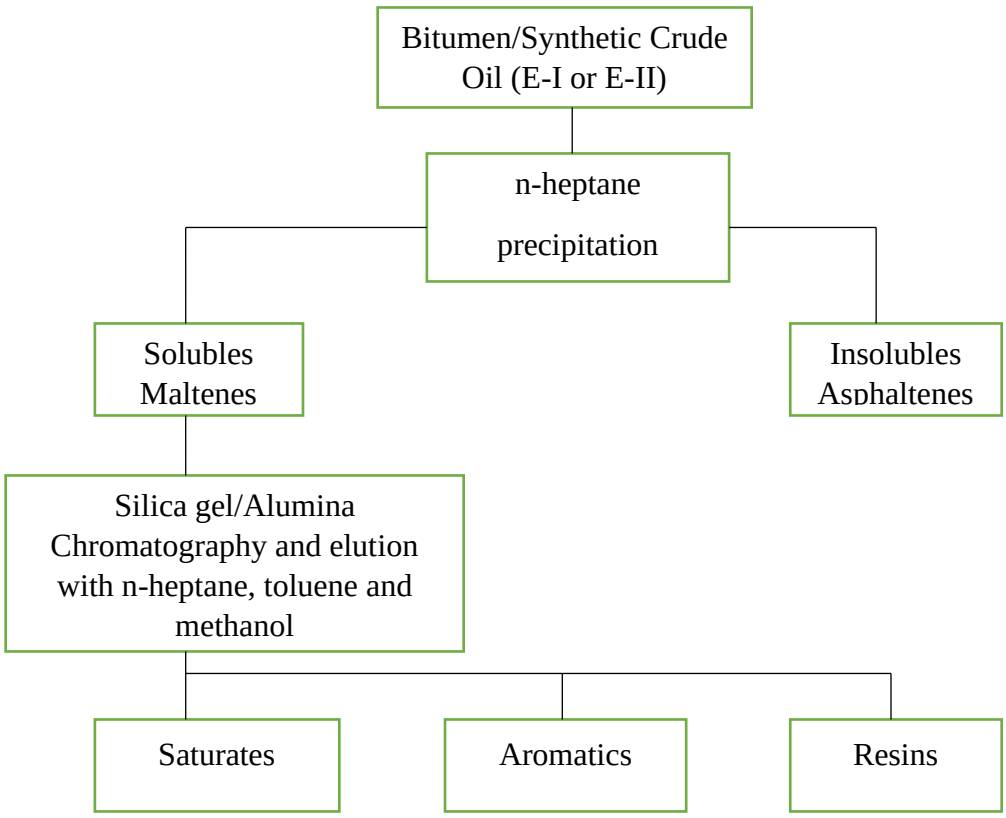

Figure 3.1: Schematic for the separation of chemical constituents in bitumen (Pomerantz *et al.*, 2013)

Plate VII: GC-MS analysis equipment (Ogundele *et al.*, 2019)

3.5 Hydrous and Anhydrous Pyrolysis

The hydrous and anhydrous pyrolysis experiment was carried out using 1200-Degree lab-scale Nitrogen atmosphere horizontal tubular furnace SA2-series manufactured by Chinese company called Samlab and supplied by Vacutec South Africa.

Plate VIII: Experimental Setup for Hydrous Pyrolysis and Anhydrous Pyrolysis (FUT Minna, Step B)

3.5.1 Anhydrous pyrolysis

For anhydrous pyrolysis, measured weights of the bitumen sample in the sample holder is placed into the furnace (Plate IX) sealed and allowed to heat up to temperatures of 200 ^{o}C, 250 ^{o}C, 300 ^{o}C, 350 ^{o}C and 400 ^{o}C each for a period of 30 minutes, 45 minutes and 60 minutes. The inert gas flow rate is set at 290 mL/minute. A schematic representation of the process is shown in Figure 3.2. After cooling and opening of the furnace and cylindrical glass tube, a thick viscous residue is obtained in the crucible (Plate X). The weight of the residue is determined and the weight of the oil (Plate XI) recovered in the conical flask is also measured before taking for further testing (Pan *et al.*, 2012).

3.5.2 Hydrous pyrolysis

For hydrous pyrolysis, measured weights of the bitumen sample plus water equivalent to 25 % weight of the bitumen poured onto the sample holder is placed into the furnace, sealed and also allowed to heat up to temperatures 200 ^{o}C, 250 ^{o}C, 300 ^{o}C, 350 ^{o}C and 400 ^{o}C each also for a period of 30 minutes, 45 minutes and 60 minutes. The inert gas flow rate is set at 290 mL/minute. After cooling and opening of the furnace and cylindrical glass tube, the weight of the residue is determined and the weight of the oil recovered in the conical flask is also measured before taking for further testing (Meredith *et al.*, 2012).

Design Expert Software was used to design both experiments and the results obtained are as reported in Tables 5 and 6.

Plate IX: Experimental setup during a run showing the inert gas flow rate of 290 mL/min (FUT Minna, Step B)

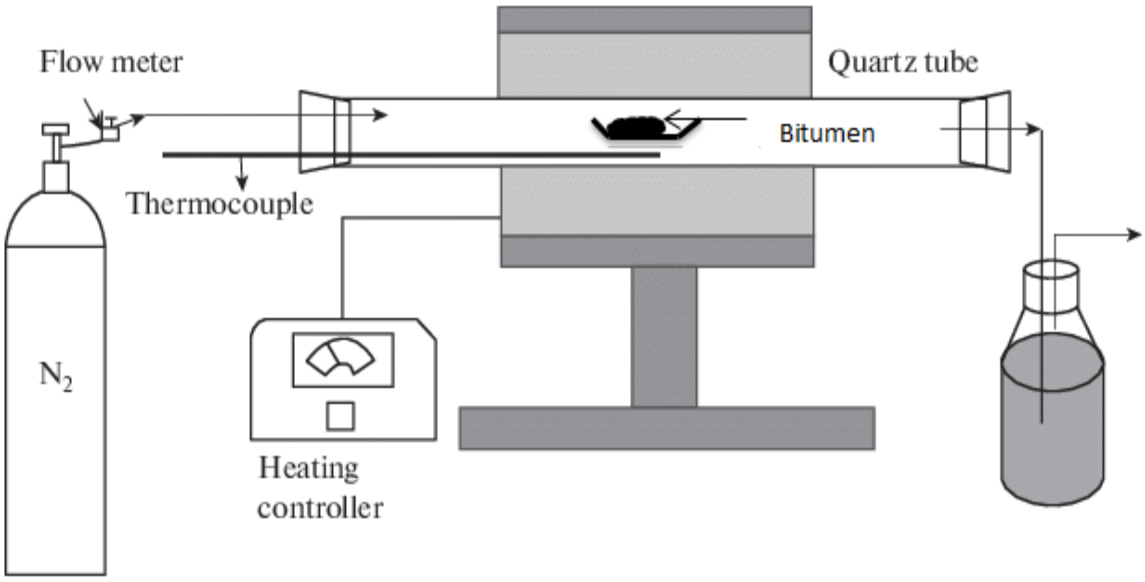

Figure 3.2: Schematic representation of how the 1200-Degree Nitrogen atmosphere horizontal tubular pyrolysis equipment functions (Lewan *et al*., 2018)

Plate X and XI show the residue from the sample holder and the synthetic crude oil respectively.

Plate X: Sample holder showing very sticky residue

Plate XI: Synthetic Crude oil yield in a sample bottle

3.6 Analysis of the Synthetic Crude Oil Yields

GC-MS analysis was also carried out on the two synthetic crude oil yields by Hydrous Pyrolysis and Anhydrous Pyrolysis in order to compare the quality of the yields including viscosity, density, specific gravity and API gravity.

3.7 Kinetic Study of the Experiment

The Coats-Redfern Method was used in the calculation of the Activation Energy and Frequency Factor.

$$\frac{d\alpha}{dt} = K(T)f(\alpha) \tag{3.2}$$

$$\alpha = \frac{m_o - m_t}{m_o - m_f} \tag{3.3}$$

$$K(T) = Aexp\left(\frac{-E_a}{RT}\right) \tag{3.4}$$

$$\frac{d\alpha}{dT} = A\ exp\left(\frac{-E_a}{RT}\right) f(\alpha) \tag{3.5}$$

$$\frac{d\alpha}{dT} = \frac{A}{\beta} exp\left(\frac{-E_a}{RT}\right) f(\alpha) \tag{3.6}$$

$$\int_0^\alpha \frac{d\alpha}{f(\alpha)} = g(\alpha) = \frac{A}{\beta}\int_{T_0}^{T} exp^{-\left(\frac{E}{RT}\right)dT} \tag{3.7}$$

and finally,

$$In\left(\frac{g(\alpha)}{T^2}\right) = In\left(\frac{AR}{\beta E}\right) - \frac{E_a}{RT} \tag{3.8}$$

where α = degree of conversion during thermal decomposition, $g(\alpha) =$ integral function of conversion, t = time, T = absolute temperature, $\frac{d\alpha}{dt} =$ the rate of conversion, $K(T) =$ temperature dependent rate constant, $f(\alpha)$ = function of reaction mechanism, m_o = initial mass of sample, m_f = mass of the sample at the end of decomposition, m_t = mass of the sample at any given time t, A = frequency factor, β = constant heating rate, R= gas constant (J/mol k) and E_a = activation energy (J/mol) (Shabbar *et al.,* 2018).

A plot of $In\left(\frac{g(\alpha)}{T^2}\right)$ against $\frac{1}{T}$ is done to give a straight line which the slope gives the activation energy and the frequency factor is calculated from the intercept. Table 3.2 below shows the

Coats-Redfern reaction order models: First-order F1, Second-order F2, and Third-order F3 (Azharul *et al.,* 2016).

Table 3.2: Coats-Redfern reaction order models (Azharul *et al.,* 2016)

Coats-Redfern reaction order models	$g(\alpha)$
First-order F1	$-\ \ln(1-\alpha)$
Second-order F2	$(1-\alpha)-1-1$
Third-order F3	$[(1-\alpha)\ -2-1]/2$

CHAPTER FOUR

4.0 RESULTS AND DISCUSSION

4.1 Determination of Viscosity, Density, Specific gravity, API gravity and Flashpoint of Bitumen

Table 4.1 highlights the properties of the bitumen sample obtained from Agbabu in Ondo state. The viscosity was determined by following ASTM D88 standard method, using a Saybolt viscometer at a Test temperature of 40 ˚C and orifice diameter 10 mm. The viscosity value of 28 cSt falls within the range of 10 cSt to 33 cSt reported by Shedrach *et al*., 2018. The density was determined following the ASTM D8188 standard method, a digital density meter, Anton-Paar was used. The density value of 0.97 g/cm^3 compares favourably with 0.88 g/cm^3 obtained at Agbabu by Onojake *et al*., 2016. The specific gravity was determined following the ASTM D5002 standard method. The specific gravity 1.01 agrees with the range of heavy oils specific gravity (Arogundade and Ogunsuyi, 2021). The API gravity 8.6 ^{o}API agrees with the range of 8.5 – 10.54 ^{o}API reported by Shedrach *et al.*, 2018 and Onojake *et al.*, 2016. The flash point value of 255 ^{o}C lies within the range 245 – 325 ^{o}C reported by Onojake *et al.*, 2016.

Table 4.1: Values of viscosity, density, specific gravity, API gravity and flash point determined for the bitumen

Properties	**Unit**	**Bitumen**
Viscosity@40 ^{o}C	cSt	28
Density	g/cm^3	0.97
Specific gravity		1.01
API gravity	^{o}API	8.6
Flash Point	^{o}C	255

4.2 Thermogravimetric Analysis TGA

The TGA for bitumen sample Figure 4.1 shows the three sections for temperature response of the bitumen. From 0 – 250 ^{o}C there is a slight drop in weight due to loss of moisture. From 280 – 400 ^{o}C there is sharp and significant decrease in weight as a result of thermal decomposition and breakdown of bitumen into subcomponents and after 400 ^{o}C there is no change observed. Figure 4.2 shows the Differential Thermal Analysis (DTA) result for the bitumen which further illustrates the three zones of temperature response of the bitumen sample with the middle zone (second zone) being significant thermal decomposition.

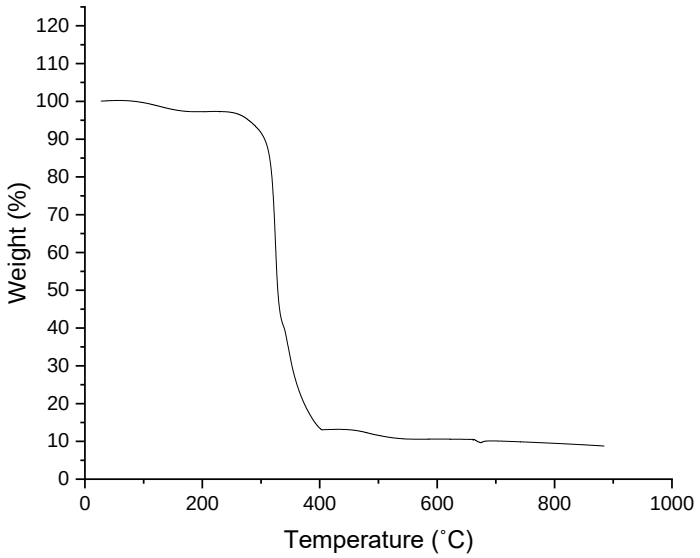

Figure 4.1: TGA for the bitumen sample at a heating rate of 10 ^{o}C /min

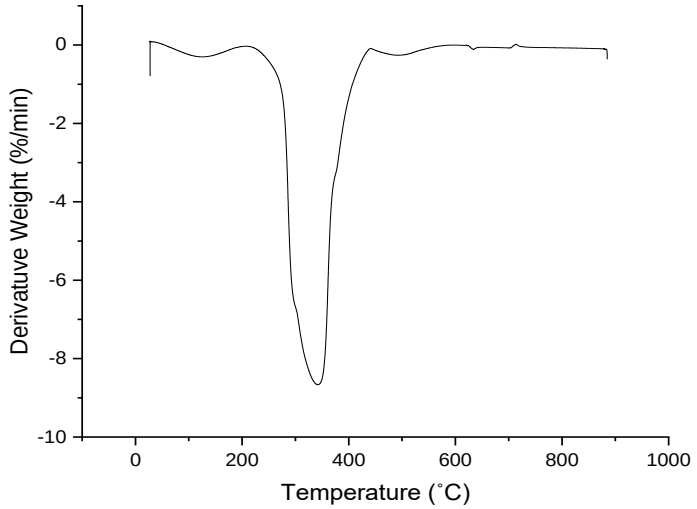

Figure 4.2: DTA for the bitumen sample

Similarly, TGA for bitumen plus water mixture Figure 4.3 shows that there is a slight change in weight from 0 – 350 ^{o}C. There is a sharp and significant weight loss observed from 370 – 500 ^{o}C which is due to thermal decomposition of the sample. Figure 4.4 shows the DTA result for bitumen water mixture which further illustrates the middle zone (second zone) being significant thermal decomposition.

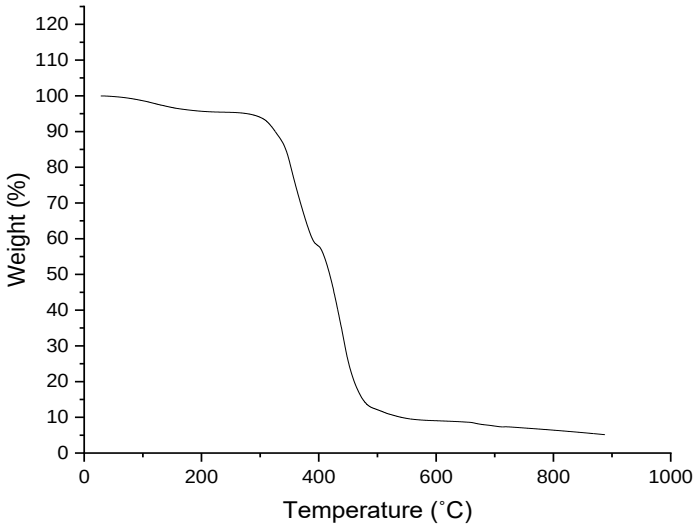

Figure 4.3: TGA to determine thermal response of bitumen plus water, also at a heating rate of 10 ^{o}C /min

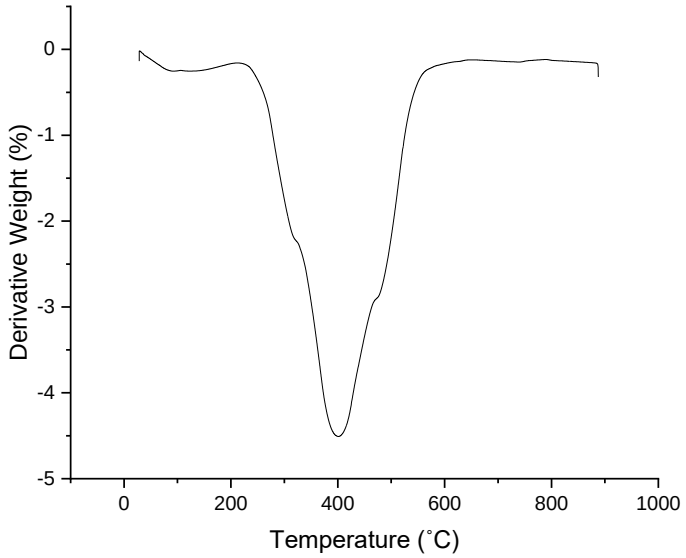

Figure 4.4: DTA for bitumen plus water

4.3 Fourier Transform Infrared Spectroscopy FT-IR

The FT-IR for the bitumen Figure 4.5 shows the peak wavelengths and Table 4.2 shows the functional groups identified at these wavelengths. The peak at 2925 cm^{-1} corresponds to the C-H bond in the CH_3 groups of alkanes and saturated hydrocarbons. The peak at 2860 cm^{-1} corresponds to C-H bond in CH_2 groups of alkanes and saturates. The peak at 1730 cm^{-1} corresponds to the C=O bond in carbonyl, carboxylic acids, alcohols and esters. The peak at 1650 cm^{-1} corresponds to the C=C bond in aromatics. The peak at 1480 cm^{-1} corresponds to the C-CH_3 groups in saturates. The peak at 1395cm^{-1} corresponds to the C-(R) groups in aromatic amines. The peak at 1050 cm^{-1} corresponds to the S=O bond in thiols, organic sulphates and sulphides. The peak at 890 cm^{-1} corresponds to the C=H bond in alkenes. The peak at 830 cm^{-1} corresponds to the functional group of para-aromatics while the peak at 770 cm^{-1} identifies functional groups of meta-aromatics and the peak at 750 cm^{-1} identifies functional group of ortho-aromatic.

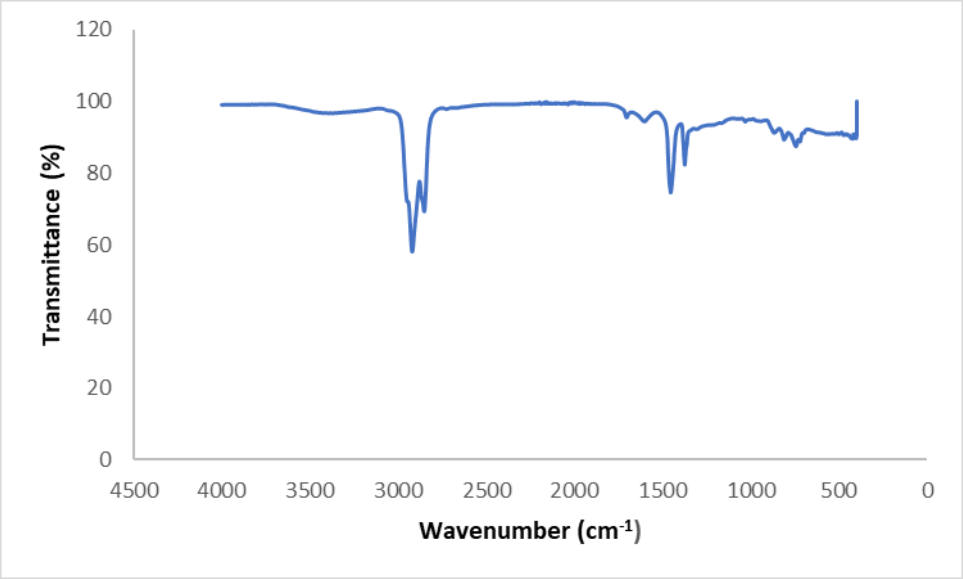

Figure 4.5: FT-IR for the bitumen sample

Table 4.2: The functional groups identified in the bitumen from the FT-IR

Peak (cm^{-1})	Bond and Functional group	Source Compound
2925	C-H Symetric stretch in CH_3	Alkane – Saturates
2860	C-H Stretch in CH_2	Alkane – Saturates
1730	C=O Stretch in carboxylic group	Carboxylic acid – Resinate
1650	C=C Stretch from Aromatic compound	Aromatics
1480	C-CH_3 Methylenic asymmetric	Alkane – Saturate
1395	C-[R] Asymmetric	Aromatic amines
1050	S=O thiols and Sulphides	Organic sulphates
890	C=H bond from alkene	Alkene – saturates
830	Two adjacent H on ring	Aromatics – para
770	Four adjacent hydrogen on ring	Aromatics – meta
750	Aromatic bending H-C modes	Aromatics – ortho

4.4 Scanning Electron Microscopy (SEM) for the Bitumen

The SEM result for the bitumen sample Figure 4.6 shows a homogeneous morphology, the whitish spots observed are due to metallic impurities which are indicated as trace elements in Table 3 from the EDX of the bitumen sample. The Carbon C, Hydrogen H, Nitrogen N, Oxygen O and Sulphur S percentage concentration are 82.3 %, 8.31 %, 3.43 %, 2.76 % and 2.16 % respectively. The trace metals V, Ni, Fe, Al, Ca, Cu, Na, Mg, Mn and Si constitute 1 % weight.

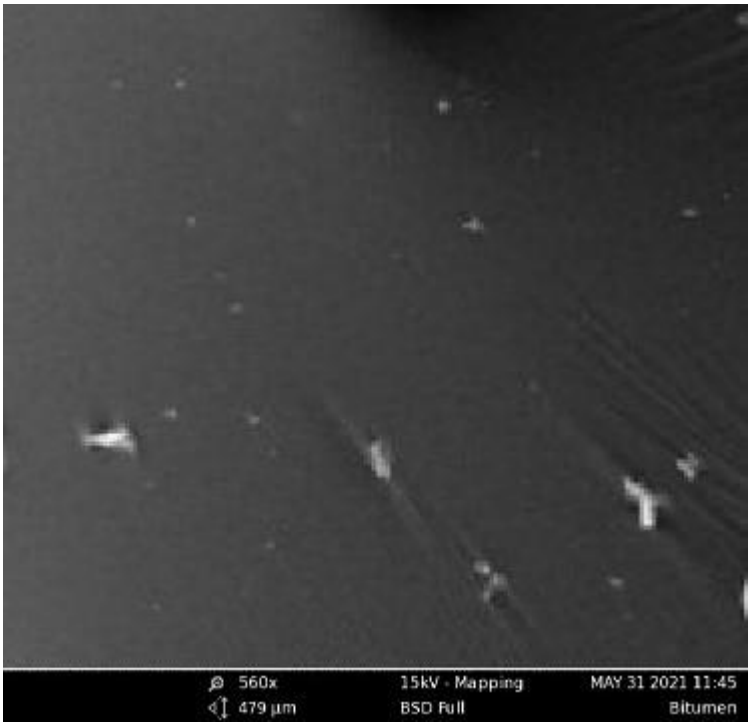

Figure 4.6: SEM morphology of the bitumen

Table 4.3: Elements identified from the Energy Dispersive X-ray Fluorescence of the bitumen

S/NO.	Element Symbol	Element Name	Weight Concentration
1	C	Carbon	82.34 %
2	H	Hydrogen	8.31 %
3	N	Nitrogen	3.43 %
4	O	Oxygen	2.76 %
5	S	Sulphur	2.16 %
6	V	Vanadium	120ppm
7	Ni	Nickel	80ppm
8	Fe	Iron	50ppm
9	Al	Aluminium	5ppm
10	Ca	Calcium	30ppm
11	Cu	Copper	5ppm
12	Na	Sodium	40ppm
13	Mg	Magnesium	20ppm
14	Mn	Manganese	22ppm
15	Si	Silicon	15ppm

4.5 XRF for the Metallic Oxides Detected in the Bitumen

The result for the XRF Table 4.4 of the oxides indicates the detection of V_2O_5, Al_2O_3, SiO_2, Na_2O, MgO, MnO, CuO, Fe_2O_3 and CaO. This corroborates with the metallic trace elements identified in the EDX.

Table 4.4: XRF of oxides detected from the bitumen sample

S/No.	Oxide	Composition ppm
1	V_2O_5	10.10
2	Al_2O_3	8.73
3	SiO_2	25.40
4	Na_2O	2.03
5	MgO	4.08
6	MnO	1.02
7	CuO	33.30
8	Fe_2O_3	13.30
9	CaO	26.04

4.6 Anhydrous Pyrolysis and Hydrous Pyrolysis Experimental Results

Table 4.5 shows the design of experiment and results obtained for the Anhydrous Pyrolysis experiment. Time and Temperature are set as the two variables; time varies from 30 – 60 minutes and temperature varies from 200 – 400 ^{o}C. The maximum yield of 4.55 g was obtained at run 12, temperature at 300 ^{o}C and time 60 minutes. Figure 4.7 shows the plot of yield for the anhydrous pyrolysis, this shows a test of fit for the actual data obtained from the laboratory process against the predicted set data from the design of experiment. 90 % of the values align correctly.

Table 4.5: Design of experiment and results of yield obtained for the anhydrous pyrolysis experiment (control experiment)

Run	Temperature (^{o}C)	Time (min)	Weight of Sample (g)	Yield (g)	Residue (g)
1	300	45	10.25	3.37	4.9
2	158.579	45	10.35	2.34	7.0
3	300	45	10.24	3.45	5.1
4	400	30	10.28	4.26	4.24
5	441.421	45	10.41	4.52	4.15
6	300	45	10.32	3.26	5.0
7	200	30	10.20	2.37	6.9
8	300	45	10.36	3.31	5.1
9	200	60	10.25	2.41	6.8
10	300	45	10.29	3.38	5.0
11	300	23.7868	10.36	3.15	5.4
12	400	60	10.21	4.55	4.18
13	300	66.2132	10.40	3.52	4.8

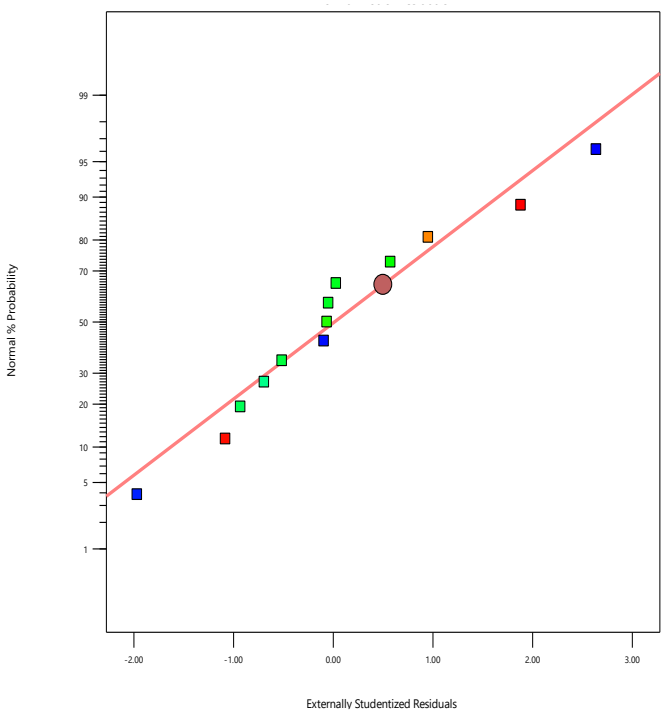

Figure 4.7: Plot of actual experimental data against predicted data for anhydrous pyrolysis

Table 4.6 also shows the design of experiment for hydrous pyrolysis experiment. The time varies from 30 – 60 minutes while temperature varies from 300 – 500 ^{o}C. The maximum yield of 5.50 g of synthetic crude is obtained at run 6 with temperature at 500 ^{o}C and time at 30minutes. Figure 4.8 shows the plot of the yield which indicates a test of fit when the actual obtained laboratory data is plotted against the predicted set data from the design of experiment. Most of the plots align except for one point which corresponds to run 5 with temperature at 300 ^{o}C and time 30 minutes.

Table 4.6: Design of experiment and results of yield obtained for the hydrous pyrolysis experiment

Run	Temperature (°C)	Time (min)	Weight of Sample (g)	Yield (g)	Residue (g)
1	300	60	12.54	3.45	8.21
2	500	60	12.51	5.30	5.85
3	400	45	12.53	4.50	6.52
4	258.579	45	12.52	2.45	8.50
5	300	30	12.53	3.40	8.02
6	500	30	12.51	5.50	5.81
7	400	23.7868	12.53	4.35	6.70
8	400	45	12.54	4.57	6.54
9	400	45	12.51	4.56	6.43
10	400	45	12.52	4.48	6.50
11	541.421	45	12.54	5.45	5.82
12	400	66.2132	12.53	4.55	6.42
13	400	45	12.52	4.60	6.41

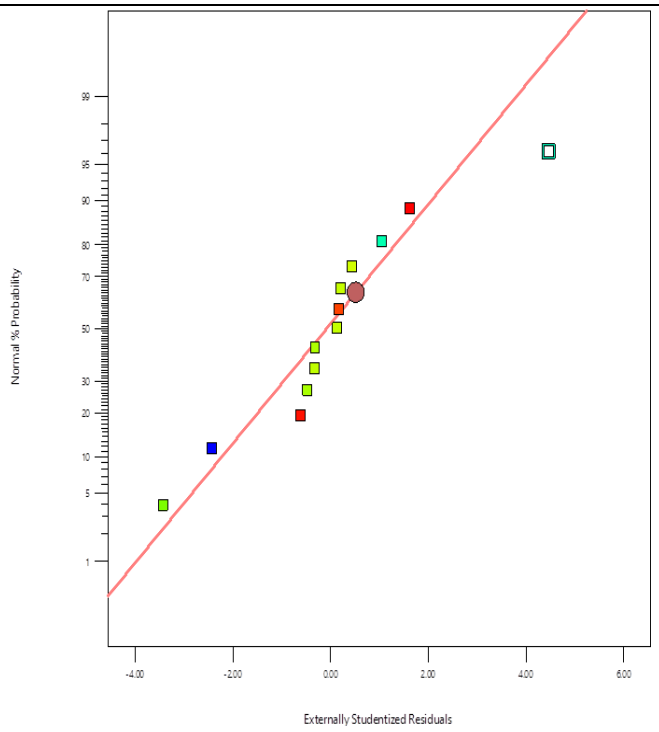

Figure 4.8: Plot of actual experimental data against predicted data for hydrous pyrolysis

4.7 GC-MS Analysis for the Bitumen and Synthetic Crude Oil Samples E-I and E-II

The GC-MS result obtained for bitumen is as shown in Table 4.7. After dissolving in n-Heptane the non-dissolvable asphaltenes constitute 2 % of the total composition while the maltenes on further elution with n-Heptane, Toluene and Methanol are saturates 35 %, aromatics 37 % and resins 26 %. These values agree with values reported by Shedrach *et al*., 2018. The chromatogram is shown in Figure 4.9.

Table 4.7: GC-MS result for the bitumen

SARA Component	Percentage (%)
Saturates	35
Aromatics	37
Resins	26
Asphaltenes	2

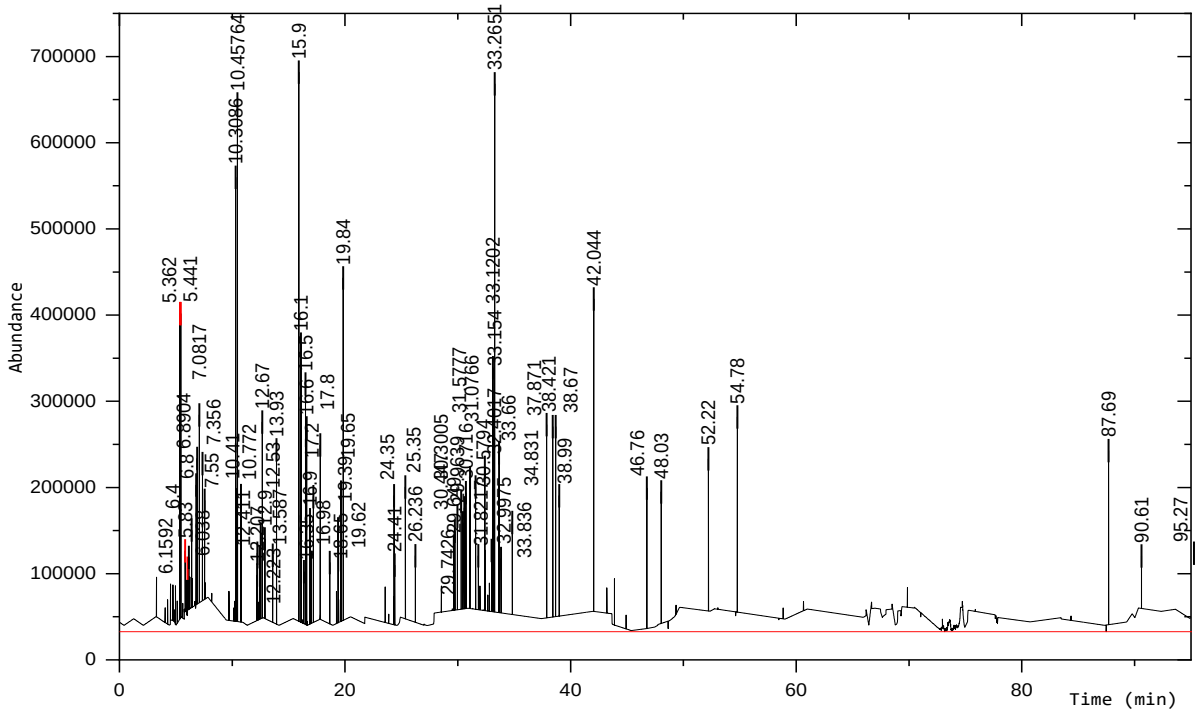

Figure 4.9: Chromatogram for GC-MS of the bitumen sample

The GC-MS result for synthetic crude oil E-I from anhydrous pyrolysis is shown in Table 4.8. After dissolving in n-Heptane and on further elution with n-Heptane, Toluene and Methanol the non-dissolvable asphaltenes constitute 0.5 %, the saturates identified constitute 50 %, aromatics 30 % and resins 19.5 %. The chromatogram is shown in Figure 4.10.

Table 4.8: GC-MS result for synthetic crude oil E-I from anhydrous pyrolysis experiment

SARA Component	Percentage (%)
Saturates	50
Aromatics	30
Resins	19.5
Asphaltenes	0.5

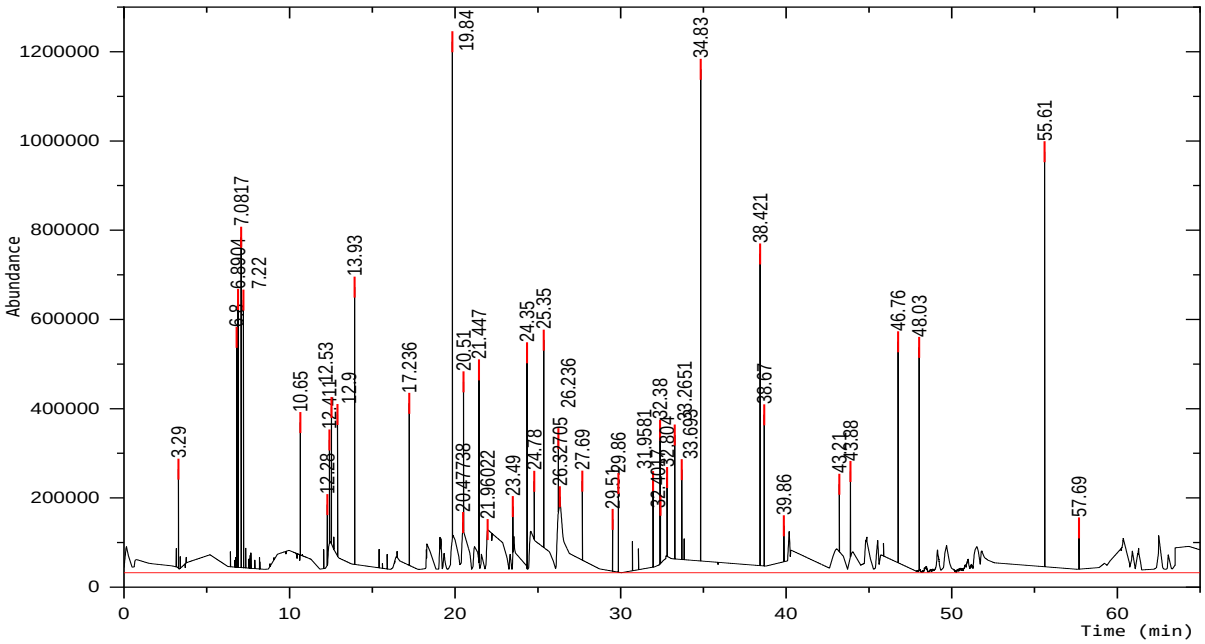

Figure 4.10: Chromatogram for GC-MS of synthetic crude oil sample E-I from anhydrous pyrolysis

The GC-MS result for synthetic crude oil E-I from anhydrous pyrolysis is shown in Table 4.9. After dissolving in n-Heptane and on further elution with n-Heptane, Toluene and

Methanol the non-dissolvable asphaltenes constitute 0.5 %, the saturates identified constitute 65 %, aromatics 25 % and resins 9.5 %. The chromatogram is shown in Figure 4.11.

Table 4.9: GC-MS result for synthetic crude oil E-II from hydrous pyrolysis experiment

SARA Component	Percentage (%)
Saturates	65
Aromatics	25
Resins	9.5
Asphaltenes	0.5

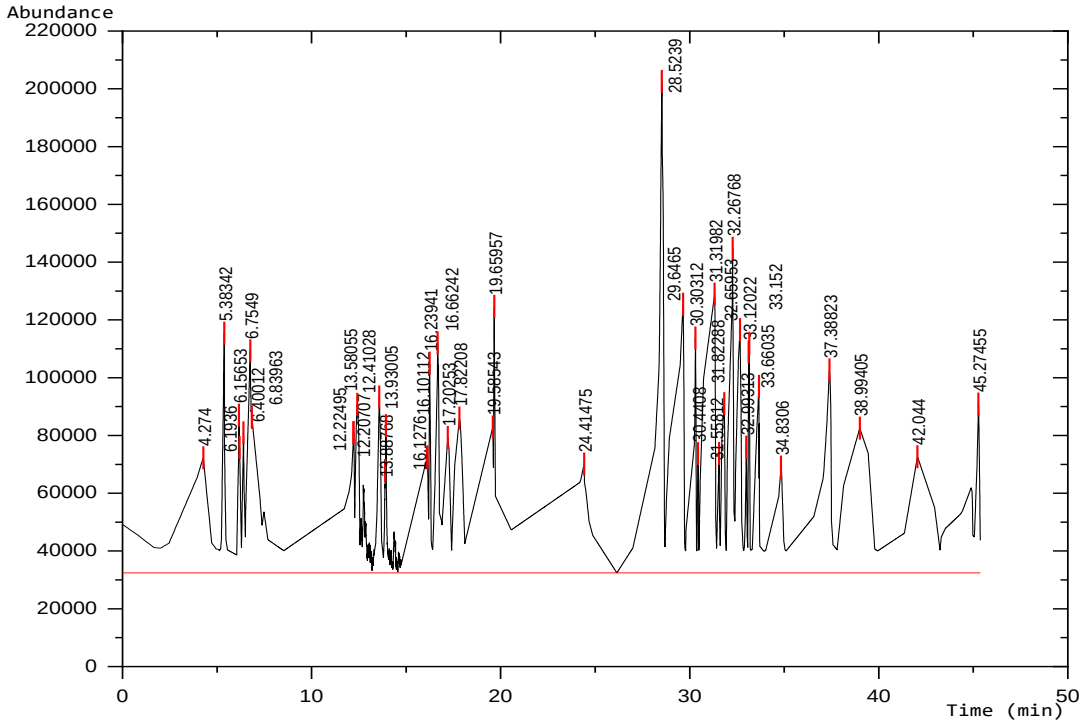

Figure 4.11: Chromatogram for GC-MS of synthetic crude oil sample E-II from hydrous pyrolysis

4.8 Viscosity, Density, Specific Gravity and API Gravity for the Synthetic Crude Oil Samples E-I and E-II

The viscosity, density, specific gravity and API gravity for the two yields are determined as reported in Table 4.10. The yield from hydrous Pyrolysis E-II is less viscous; it has lower

density, lower specific gravity and therefore higher API gravity of 29.2 ^{o}API. Also the flash point from the yield from hydrous pyrolysis is lower than the flash point of the yield from anhydrous pyrolysis. The two synthetic crude oil yields are compared to standard crude Bonny Light and by API gravity the yield from hydrous pyrolysis is closer to standard and therefore light crude.

Table 4.10: Values obtained for the determination of physicochemical properties of both synthetic crude oil samples compared to standard Bonny Light crude

Properties	Unit	Sample E-I	E-II	Bonny Light
Density	g/cm^3	0.89	0.87	0.83
Specific gravity		0.91	0.88	0.86
API gravity	^{o}API	23.99	29.20	32.9
Viscosity(@40^{o}C)	cSt	3.28	3.04	4.35
Flash Point	^{o}C	98	78	35

4.9 Calculation of Activation Energy and Frequency Factor

As calculated from kinetic data values using Coats-Redfern relation, Tables 4.11 and 4.12, the activation energy for hydrous pyrolysis is 224.04 $kJmol^{-1}$ and the frequency factor is 1.253×10^{17} s^{-1}. The activation energy and frequency factor for anhydrous pyrolysis is 291.796 $kJmol^{-1}$ and 9.645×10^{24} s^{-1} respectively. Hydrous pyrolysis has lower activation energy; this indicates that hydrous pyrolysis is the dominant mechanism for the pyrolysis and it occurs at a much faster rate than anhydrous pyrolysis.

Table 4.11: Results for kinetic data of anhydrous pyrolysis

T(ºC)	A	1 – α	g (α)	T + 273 (K)	T^2	1/T	ln [g(α)/T^2]
309.13	0.100187	0.899813	0.105569	582.13	338875.3	0.001718	-14.9818
318.4	0.201147	0.798853	0.224579	591.4	349754	0.001691	-14.2585
322.04	0.303898	0.696102	0.362259	595.04	354072.6	0.001681	-13.7927
324.53	0.405537	0.594463	0.520096	597.53	357042.1	0.001674	-13.4394
326.94	0.505162	0.494838	0.703525	599.94	359928	0.001667	-13.1453
330.76	0.600023	0.399977	0.916349	603.76	364526.1	0.001656	-12.8937
343.12	0.700293	0.299707	1.204949	616.12	379603.9	0.001623	-12.6604
354.28	0.800819	0.199181	1.613543	627.28	393480.2	0.001594	-12.4044
372.36	0.900152	0.099848	2.304108	645.36	416489.5	0.00155	-12.1049
490.09	1	0		763.09	582306.3	0.00131	

As shown in the graph Figure 4.12, the Activation Energy is calculated from the slope while Frequency Factor is calculated from the intercept.

The Activation Energy and Frequency Factor are calculated as:

Ea = 291.796 $kJmol^{-1}$ and A = 9.645 x 10^{24} s^{-1}

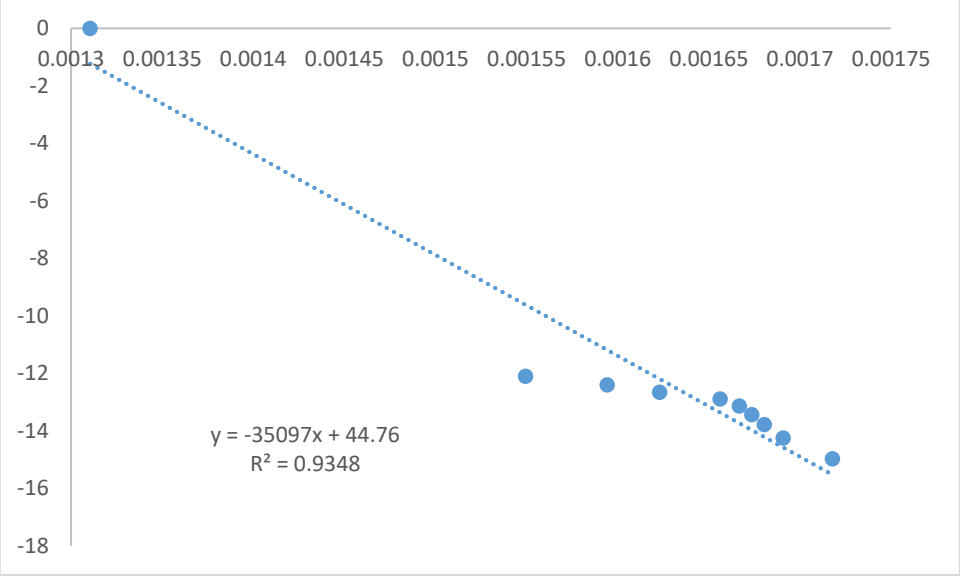

Figure 4.12: Kinetic plot for anhydrous pyrolysis

Similarly, for hydrous pyrolysis;

From the Coats-Redfern relation, the results obtained for the calculation of kinetic data are shown in Table 4.12 below.

Table 4.12: Results for kinetic data of hydrous pyrolysis

T(ºC)	α	1 – α	g (α)	T + 273 (K)	T^2	1/T	ln [g(α)/T^2]
338.89	0.100274	0.899726	0.105665	611.89	374409.4	0.001634	-15.0806
355.41	0.200941	0.799059	0.224321	628.41	394899.1	0.001591	-14.3811
369.75	0.300774	0.699226	0.357782	642.75	413127.6	0.001556	-13.9593
386.7	0.4007	0.5993	0.511993	659.7	435204.1	0.001516	-13.653
414.78	0.500684	0.499316	0.694516	687.78	473041.3	0.001454	-13.4315
427.75	0.600401	0.399599	0.917294	700.75	491050.6	0.001427	-13.1906
438.8	0.700756	0.299244	1.206495	711.8	506659.2	0.001405	-12.9479
449.22	0.801064	0.198936	1.614773	722.22	521601.7	0.001385	-12.6855
466.08	0.900202	0.099798	2.304604	739.08	546239.2	0.001353	-12.3759
585.14	1	0		858.14	736404.3	0.001165	

As shown in the plot Figure 4.13, the Activation Energy is calculated from the slope while Frequency Factor is calculated from the intercept

The Activation Energy and Frequency Factor are calculated as:

Ea = 224.04 $kJmol^{-1}$ and A = 1.253 x 10^{17} s^{-1}

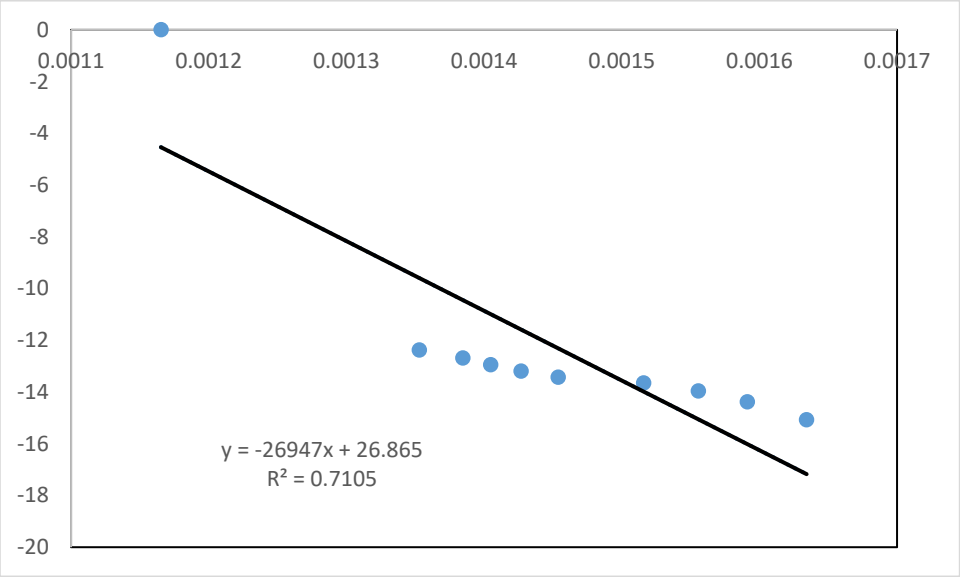

Figure 4.13: Kinetic plot for hydrous pyrolysis

CHAPTER FIVE

5.0 CONCLUSION AND RECOMMENDATION

5.1 Conclusion

a. The bitumen was characterized and the viscosity was determined to be 28 cSt, the density was determined to be 0.97 g/cm^3 and the specific gravity was determined to be 1.01.

b. Anhydrous pyrolysis was carried out on the bitumen and the maximum yield of 4.55 g was obtained at run 12 with temperature 300 ^{o}C for 60 minutes.

c. Hydrous pyrolysis was carried out on the bitumen and the maximum yield of 5.50 g was obtained at run 6 with temperature 500 ^{o}C for 30 minutes.

d. GC-MS analysis showed that the synthetic crude oil yield E-II from hydrous pyrolysis had 65 % concentration of saturates which was more than the 50 % saturates from the synthetic crude oil yield E-I obtained from anhydrous pyrolysis.

e. Kinetics study using Coats-Redfern method showed that the lower activation energy 224.04 kJmol^{-1} for hydrous pyrolysis compared to 291.796 kJmol^{-1} for anhydrous pyrolysis indicated that hydrous pyrolysis was the dominant mechanism for the pyrolysis and it occurred at a much faster rate than anhydrous pyrolysis.

5.2 Recommendation

It is recommended that further research should be carried out on the micro analysis of both processes in order to study the kinetics of these processes further and help with equipment design for the continuous exploration of bitumen in future.

5.3 Contribution to Knowledge

a. Kinetic study of the hydrous pyrolysis was carried out on the bitumen which prior to this research, there was little or no information about the kinetics of hydrous pyrolysis of Bitumen.

b. The Activation Energy and Frequency Factor for hydrous pyrolysis of the Bitumen sample were calculated respectively as 224.04 $kJmol^{-1}$ and 1.253 x 10^{17} $s^{-1.}$ While the Activation Energy and Frequency Factor for anhydrous pyrolysis of the Bitumen were calculated respectively as 291.796 $kJmol^{-1}$ and 9.645 x 10^{24} s^{-1}.

REFERENCES

Arogundade, L. O & Ogunsuyi, H. O. (2021). Microstructural and Functional group analysis of Polyphosphoric Acid-Modified Natural Bitumen. *International Journal of Scientific & Engineering Research*, Vol. 12, Issue 3, p. 721 – 727.

Azharul, M. I., Auta, M., Kabir, G. & Hameed B. H. (2016). A thermogravimetric analysis of the combustion kinetics of karanja (Pongamia pinnata) fruit hulls char. *Elsevier, Journal of Bioresource Technology*, 200, p. 335-341.

Behar, F., Vandenbroucke, M., Tang, Y., Marquis, F., & Espitalie, J. (2007). Thermal cracking of kerogen in open and closed systems: Determination of kinetic parameters and stoichiometric coefficients for oil and gas generation. *Organic Geochemistry*, 26, p. 321-339.

Berwick, L.J., Greenwood, P.F., Meredith, W., Snape, C.E., & Talbot, H.M. (2017). Comparison of microscale sealed vessel pyrolysis (MSSVpy) and hydropyrolysis (Hypy) for the characterisation of extant and sedimentary organic matter. *Journal of Analytical and Applied Pyrolysis*, 87, p. 108-116.

Carr, A.D., Snape, C.E., Meredith, W., Uguna, C., Scotchman, I.C., & Davis, R.C. (2009). The effect of water pressure on hydrocarbon generation reactions: Some inferences from laboratory experiments. *Petroleum Geoscience*, 15, p. 17-26.

Czarnecka, E., & Gillott, J.E. (2000). Formation and characterization of clay characterization of clay complexes with bitumen from Athabasca oil sand. *Clays and Clay Minerals*, 28, p. 197-203.

Durand, B. (2003). A history of organic geochemistry. *Oil and Gas Science and Technology*, 58, p. 203-231.

Eglinton, T.I., Rowland, S.J., Curtis, C.D., & Douglas, A.G. (2006). Kerogen-mineral reactions at raised temperatures in the presence of water. *Organic Geochemistry*, 10, p. 1041-1052.

Evans, C.R., Rogers, M.A., & Baily, N.J.L. (2001). Evolution and alteration of petroleum in Western Canada. *Chemical Geology*, 8, p. 147-170.

Freund, H., Clouse, J.A., & Otten, G.A. (2003). Effect of pressure on the kinetics of kerogen pyrolysis. *Energy & Fuels*, 7, p. 1088-1094.

Greenfield, M.L., Byrne, M., Mitra-Kirtley, S., Kercher, E.M., Bolin, T.B., & Wu, T. (2015). XANES measurements of sulfur chemistry during asphalt oxidation. *Energy & Fuels*, 10, p. 364 – 378.

Hart, A. (2012). The catalytic upgrading of heavy crude oil in-situ: the role of hydrogen: a review. *International Journal of Petroleum Science and Technology*, p.79. *GaleAcademicOneFile*, link.gale.com/apps/doc/A323659176/AONE?u=anon~ed8974f1&sid=googleScholar&xid=082368f4. Accessed 2nd Aug. 2021.

Hoering, T.C. (2004). Thermal reactions of kerogen with added water, heavy water and pure organic substances. *Organic Geochemistry*, 5, p. 267-278.

Kelemen, S.R., George, G.N., Hackett, M.J., Sansone, M., Gorbaty, M.L., Kelemen, S.R., & Prince, R.C. (2014). Long-range chemical sensitivity in the sulfur K-edge X-ray absorption spectra of substituted thiophenes. *J. Physical Chemistry*, 8, p. 523 – 545.

Kelemen, S.R., Walters, C.C., Kwiatek, P.J., Freund, H., Afeworki, M., & Sansone, M. (2010). Characterization of solid bitumens originating from thermal chemical alteration and thermochemical sulfate reduction. *Geochimical et Cosmochimica Acta*, 38, p. 155 – 243.

Knauss, K.G., Copenhaver, S.A., Braun, R.L., & Burnham, A.K. (2007). Hydrous pyrolysis of New Albany and Phosphoria shales: Production kinetics of carboxylic acids and light hydrocarbons and interactions between the inorganic and organic chemical systems. *Organic Geochemistry*, 27, p. 477-496.

Lewan, M., Justin, E., Kyle, D., Paul, R., Andrew, E., & Julia, C. (2018). Evolution of sulfur speciation in bitumen through hydrous pyrolysis induced thermal maturation of Jordanian Ghareb Formation oil shale. *Energy & Fuels* 2, p. 50-53.

Lewan, M.D. (2002). Water as a source of hydrogen and oxygen in petroleum formation by hydrous pyrolysis. *American Chemical Society*, Division of Fuel Chemistry Preprints, 37, p. 164-169.

Mcnab, J.D., Smith, P.V., & Betts, R.L. (2002). The evolution of petroleum. *Industrial and Engineering Chemistry*, 44, p. 255-256.

Meredith, W., Carr, A.D., Snape, C.E., Uguna, C.N., & Castro-Díaz, M. (2012). A Laboratory pyrolysis study to investigate the effect of water pressure on hydrocarbon generation and maturation of coals in geological basins. *Organic Geochemistry*, 52, p. 103–113.

Michels, R., Landais, P., Philip, R.P., & Torkelson, B.E. (2004). Effects of pressure on organic matter maturation during confined pyrolysis of Woodford kerogen. *Energy & Fuels*, 8, p. 741-754.

Michels, R., Landais, P., Torkelson, B.E., & Philip, R.P. (2005). Effects of effluents and water pressure on oil generation during confined pyrolysis and high-pressure hydrous pyrolysis. *Geochimical et Cosmochimica Acta*, 59, p. 158-164.

Mitra-Kirtley, S., Mullins, O.C., & Pomerantz, A.E. (2016). Sulfur and nitrogen chemical speciation in crude oils and related carbonaceous materials. *Engineering Science*, 12, p. 52 – 57.

Monthioux, M., Landais, P., & Durand, B. (2006). Comparison between extracts from natural and artificial maturation series of Mahakam Delta coals. *Organic Chemistry*, 10, p. 299-311.

Ogundele, O. D., Thompson, S. O., Jayeola, J. O., & Olansile A. O. (2019). Gas Chromatography-Mass Spectrometry Analysis of Chromatographic Fractions of Nigerian Bitumen. *International Journal of Current Research in Applied Chemistry & Chemical Engineering*, Vol. 3, Issue 1, p. 31 – 38.

Ogunsuyi, H. O., Olubode, O. A., & Toluwalope, A. (2011). Chemical analysis of Agbabu Bitumen Exudate as potential refinery feedstock. *Journal of Applied Science and Technology*, 16(1-2). DOI:10.4314/jast.v16i1-2.64785.

Ojeyemi, M. O., Akintomiwa, O. E., & Hassan, O. B. (2015). Preliminary Investigation on Modification of Agbabu Natural Bitumen with Some Polymeric Materials. *International Journal of Scientific & Engineering Research*, Vol. 6, Issue 9, p. 1342 – 1347.

Onojake, M.C., & Ndubuka, C.O. (2016). Appraisal of the Bulk Properties of Bitumen Samples from Four Deposits in South West, Nigeria. *Petroleum & Coal*, Vol. 58, p. 407– 413.

Pan, C.C., Geng, A.S., Zhong, N.N., Liu, J.Z., & Yu, L.P. (2012). Kerogen pyrolysis in the presence and absence of water and minerals: amounts and compositions of bitumen and liquid hydrocarbons. *Petroleum & Coal*, Vol. 36, p. 27–33.

Peters, K.E., Moldowan, J.M., & Sundararaman, P. (2000). Effects of hydrous pyrolysis on biomarker thermal maturity parameters: Monterey Phosphatic and Siliceous members. *Organic Geochemistry*, 15, p. 249-265.

Pomerantz, A.E., Seifert, D.J., Bake, K.D., Craddock, P.R., Mullins, O.C., & Kodalen B.G. (2013). Sulfur chemistry of asphaltenes from a highly compositionally graded oil column. *Energy & Fuels* 15, p. 243-255.

Price, L.C., & Wenger, L.M. (2012). The influence of pressure on petroleum generation and maturation as suggested by aqueous pyrolysis. *Organic Geochemistry*, 19, p. 141-159.

Shabbar, S., Rana, Q., Ilham T., & Isam J. (2018). Kinetics of pyrolysis and combustion of oil shale sample from thermogravimetric data. *Energy & Fuels*, 6, p. 521-648.

Shedrach, O. O., Jennifer, O. A., Adeyinka, S. Y., & Victor, A. (2018). Physical Properties of Agbabu and Yegbata Bitumen in Nigeria. *Journal of Applied Science & Process Engineering*, Vol. 5, No. 1, p. 227 – 240.

Speight, J.G. (2009). *The chemistry and technology of petroleum*. New York, Marcel Dekker Inc., p. 32 - 37.

Stainforth, J.G. (2009). Practical kinetic modelling of petroleum generation and expulsion. *Marine and Petroleum Geology*, 26, p. 552-572.

Tissot, B.P., & Welte, D.H. (2004). *Petroleum formation and occurrence*. Berlin, Springer-Verlag Inc., p. 24 - 36.

Uguna, C.N., Carr, A.D., Snape, C.E., Meredith, W., & Castro-Díaz, M. (2012). A laboratory pyrolysis study to investigate the effect of water pressure on hydrocarbon generation and maturation of coals in geological basins. *Organic Geochemistry*, 52, p. 103-113.

Van Graas, G., de Leeuw, J.W., Schenck, P.A., & Haverkamp, J. (2001). Kerogen of Toarcian shales of the Paris basin. A study of its maturation by flash pyrolysis techniques. *Geochimica et Cosmochimica Acta*, 45, p. 246-274.

Wampler, T.P. (2007). *Applied pyrolysis handbook*. Boca Raton, London, New York, Taylor & Francis Group, p. 77 – 83.

APPENDICES

A1: Calculation of Activation energy for Bitumen (anhydrous) pyrolysis

From the Coats-Redfern Equation (eq. 3.7), the kinetic data calculated for the Coats-Redfern First-order (F1) reaction model are as shown in Table 4.11.

As shown in Figure 4.12

y = -35097x + 44.76

$\frac{-E_\alpha}{R}$ = -35097

$E\alpha$ = 35097 × 8.314

= 291796.458

≈ 291.796 kJmol^{-1}

$In\left(\frac{AR}{\beta E}\right)$ = 44.76

$A = \frac{e^{44.76} \times 10 \times 291796.458}{8.314}$

= 9.645 × 10^{24} s^{-1}

For the Second-order (F2) reaction model for bitumen pyrolysis, the calculated kinetic data are as shown in Table A.1

Table A.1: Kinetic data for Coats-Redfern second-order (F2) reaction model for bitumen pyrolysis

T(ºC)	A	1 – α	g (α)	T + 273 (K)	T^2	1/T	ln |[g(α)/T^2]|
309.13	0.100187	0.899813	-1.10019	582.13	338875.3	0.001718	-12.6379
318.4	0.201147	0.798853	-1.20115	591.4	349754	0.001691	-12.5817
322.04	0.303898	0.696102	-1.3039	595.04	354072.6	0.001681	-12.5119
324.53	0.405537	0.594463	-1.40554	597.53	357042.1	0.001674	-12.4452
326.94	0.505162	0.494838	-1.50516	599.94	359928	0.001667	-12.3848
330.76	0.600023	0.399977	-1.60002	603.76	364526.1	0.001656	-12.3363
343.12	0.700293	0.299707	-1.70029	616.12	379603.9	0.001623	-12.3161
354.28	0.800819	0.199181	-1.80082	627.28	393480.2	0.001594	-12.2945
372.36	0.900152	0.099848	-1.90015	645.36	416489.5	0.00155	-12.2977
490.09	1	0	-2	763.09	582306.3	0.00131	-12.5816

The term ln[g(α)/T^2] gives an error value, hence the plot of ln[g(α)/T^2] against 1/T cannot be made and the Activation energy cannot be calculated for the Coats-Redfern second-order

reaction model. This confirms that the bitumen pyrolysis is a first order reaction (however, the absolute value is imputed as ln $|[g(\alpha)/T^2]|$ in Table A.1 above).

For the Third-order (F3) reaction model, the calculated kinetic data are as shown in Table A.2

Table A.2: Kinetic data for Coats-Redfern third-order (F3) reaction model

T(ºC)	A	1 – α	g (α)	T + 273 (K)	T^2	1/T	ln $\|[g(\alpha)/T^2]\|$
309.13	0.100187	0.899813	-1.05009	582.13	338875.3	0.001718	-12.6845
318.4	0.201147	0.798853	-1.10057	591.4	349754	0.001691	-12.6692
322.04	0.303898	0.696102	-1.15195	595.04	354072.6	0.001681	-12.6358
324.53	0.405537	0.594463	-1.20277	597.53	357042.1	0.001674	-12.601
326.94	0.505162	0.494838	-1.25258	599.94	359928	0.001667	-12.5685
330.76	0.600023	0.399977	-1.30001	603.76	364526.1	0.001656	-12.544
343.12	0.700293	0.299707	-1.35015	616.12	379603.9	0.001623	-12.5467
354.28	0.800819	0.199181	-1.40041	627.28	393480.2	0.001594	-12.546
372.36	0.900152	0.099848	-1.45008	645.36	416489.5	0.00155	-12.568
490.09	1	0	-1.5	763.09	582306.3	0.00131	-12.8693

The term $\ln[g(\alpha)/T^2]$ gives an error value, hence the plot of $\ln[g(\alpha)/T^2]$ against 1/T cannot be made and the Activation energy cannot be calculated for the Coats-Redfern third-order reaction model. This further confirms that the bitumen pyrolysis is a first order reaction (however, the absolute value is imputed as ln $|[g(\alpha)/T^2]|$ in Table A.2 above).

A2: Calculation of Activation energy for Bitumen water mixture (hydrous) pyrolysis

From the Coats-Redfern Equation (eq. 3.7), the kinetic data calculated for the Coats-Redfern First-order (F1) reaction model are as shown in Table 4.12.

As shown in Figure 4.13

$Y = 26947x + 26.865$

$\frac{-E\alpha}{R} = -26947$

$E\alpha = 26947 \times 8.314$

$= 224037.358$

$\approx 224.04\ \text{kJmol}^{-1}$

$$In\left(\frac{AR}{\beta E}\right) = 26.865$$

$$\frac{AR}{\beta E} = e^{26.865}$$

$$\mathrm{A} = \frac{e^{26.865} \times 10 \times 224037.358}{8.314}$$

$$= 1.253 \times 10^{17} s^{-1}$$

For the Second-order (F2) reaction model for bitumen water mixture pyrolysis, the calculated kinetic data are as shown in Table A.3

Table A.3: Kinetic data for Coats-Redfern second-order (F2) reaction model for bitumen water mixture pyrolysis

T(°C)	A	1 - α	g (α)	T + 273 (K)	T^2	1/T	ln |[g(α)/T^2]|
338.89	0.100274	0.899726	-1.10027	611.89	374409.4	0.001634	-12.7375
355.41	0.200941	0.799059	-1.20094	628.41	394899.1	0.001591	-12.7033
369.75	0.300774	0.699226	-1.30077	642.75	413127.6	0.001556	-12.6686
386.7	0.4007	0.5993	-1.4007	659.7	435204.1	0.001516	-12.6466
414.78	0.500684	0.499316	-1.50068	687.78	473041.3	0.001454	-12.661
427.75	0.600401	0.399599	-1.6004	700.75	491050.6	0.001427	-12.634
438.8	0.700756	0.299244	-1.70076	711.8	506659.2	0.001405	-12.6045
449.22	0.801064	0.198936	-1.80106	722.22	521601.7	0.001385	-12.5763
466.08	0.900202	0.099798	-1.9002	739.08	546239.2	0.001353	-12.5689
585.14	1	0	-2	858.14	736404.3	0.001165	-12.8164

The term $\ln[g(\alpha)/T^2]$ gives an error value, hence the plot of $\ln[g(\alpha)/T^2]$ against 1/T cannot be made and the Activation energy cannot be calculated for the Coats-Redfern second-order reaction model. This confirms that the bitumen water mixture pyrolysis is a first order reaction (however, the absolute value is imputed as $\ln |[g(\alpha)/T^2]|$ in Table A.3 above).

For the Third-order (F3) reaction model for bitumen water mixture pyrolysis, the calculated kinetic data are as shown in Table A.4

Table A.4: Kinetic data for Coats-Redfern third-order (F3) reaction model for bitumen water mixture pyrolysis

T(°C)	A	1 – α	g (α)	T + 273 (K)	T^2	1/T	ln |[g(α)/T^2]|
338.89	0.100274	0.899726	-1.05014	611.89	374409.4	0.001634	-12.7842
355.41	0.200941	0.799059	-1.10047	628.41	394899.1	0.001591	-12.7906
369.75	0.300774	0.699226	-1.15039	642.75	413127.6	0.001556	-12.7914
386.7	0.4007	0.5993	-1.20035	659.7	435204.1	0.001516	-12.801
414.78	0.500684	0.499316	-1.25034	687.78	473041.3	0.001454	-12.8435
427.75	0.600401	0.399599	-1.3002	700.75	491050.6	0.001427	-12.8418
438.8	0.700756	0.299244	-1.35038	711.8	506659.2	0.001405	-12.8352
449.22	0.801064	0.198936	-1.40053	722.22	521601.7	0.001385	-12.8278
466.08	0.900202	0.099798	-1.4501	739.08	546239.2	0.001353	-12.8392
585.14	1	0	-1.5	858.14	736404.3	0.001165	-13.1041

The term $\ln[g(\alpha)/T^2]$ gives an error value, hence the plot of $\ln[g(\alpha)/T^2]$ against 1/T cannot be made and the Activation energy cannot be calculated for the Coats-Redfern third-order reaction model. This further confirms that the bitumen water mixture pyrolysis is a first order reaction (however, the absolute value is imputed as $\ln|[g(\alpha)/T^2]|$ in Table A.4 above).

A.3 Calculation of specific gravity (relative density)

Table A.5 shows the weights measured in the determination of specific gravity.

Table A.5: Weights measured in the determination of specific gravity.

Parameter	Value (g)
Weight of empty beaker	25.4
Weight of beaker and distilled water	50.95
Weight of beaker and bitumen sample	51.24

Let M_w, M_B and M_b be the weight of water, bitumen and empty beaker respectively.

Let V_w, V_B and V_b be the volume of water, bitumen and beaker respectively.

Let ρ_w and ρ_B be the density of water and bitumen respectively

M_w = weight of (beaker and water – empty beaker) = 50.95 – 25.4 = 25.55 g

M_B = weight of (beaker and bitumen sample – empty beaker) = 51.24 – 25.4 = 25.84 g

Given, ρ_w = 1 g/cm^3 (constant)

Volume of beaker is constant, therefore

$V_b = V_w = V_B$ since the same beaker was used for both water and the bitumen sample

$V_w = \frac{M_w}{\rho_w} = \frac{25.55}{1}$ = 25.55 cm^3

Thus, $V_w = V_B$ = 25.55 cm^3

Therefore, $V_B = \frac{M_B}{\rho_B} = \frac{25.84}{\rho_B}$

$$25.55 = \frac{25.84}{\rho_B}$$

$$\rho_B = \frac{25.84}{25.55} = 1.0114 \text{ g/cm}^3$$

Hence, specific gravity of bitumen = $\frac{\rho_B}{\rho_w} = \frac{1.0114}{1}$ = 1.0114

Specific gravity of bitumen = 1.01